

# Can AI Dream of Unseen Galaxies? Conditional Diffusion Model for Galaxy Morphology Augmentation

CHENRUI MA <sup>1</sup>, ZECHANG SUN <sup>2</sup>, TAO JING <sup>2</sup>, ZHENG CAI <sup>2</sup>, YUAN-SEN TING <sup>3,4</sup>, SONG HUANG <sup>2</sup>, AND  
MINGYU LI <sup>2</sup>

<sup>1</sup>*Tsinghua Shenzhen International Graduate School, Tsinghua University, Shenzhen China*

<sup>2</sup>*Department of Astronomy, Tsinghua University, Beijing China*

<sup>3</sup>*The Ohio State University, Columbus, OH 43210, USA*

<sup>4</sup>*Center for Cosmology and AstroParticle Physics (CCAPP), The Ohio State University, Columbus, OH 43210, USA*

## ABSTRACT

Observational astronomy relies on visual feature identification to detect critical astrophysical phenomena. While machine learning (ML) increasingly automates this process, models often struggle with generalization in large-scale surveys due to the limited representativeness of labeled datasets—whether from simulations or human annotation—a challenge pronounced for rare yet scientifically valuable objects. To address this, we propose a conditional diffusion model to synthesize realistic galaxy images for augmenting ML training data. Leveraging the Galaxy Zoo 2 dataset which contains visual feature – galaxy image pairs from volunteer annotation, we demonstrate that our model generates diverse, high-fidelity galaxy images closely adhere to the specified morphological feature conditions. Moreover, this model enables generative extrapolation to project well-annotated data into unseen domains and advancing rare object detection. Integrating synthesized images into ML pipelines improves performance in standard morphology classification, boosting completeness and purity by up to 30% across key metrics. For rare object detection, using early-type galaxies with prominent dust lane features ( $\sim 0.1\%$  in GZ2 dataset) as a test case, our approach doubled the number of detected instances—from 352 to 872—compared to previous studies based on visual inspection. This study highlights the power of generative models to bridge gaps between scarce labeled data and the vast, uncharted parameter space of observational astronomy and sheds insight for future astrophysical foundation model developments. Our project homepage is available at <https://galaxysd-webpage.streamlit.app/>.

**Keywords:** Diffusion Model — Galaxy Morphology — Machine Learning

## 1. INTRODUCTION

Modern astronomy increasingly relies on accurate and robust machine learning (ML) systems to efficiently process vast observational datasets (e.g., Ball et al. 2006; Speagle et al. 2019b; Ting et al. 2019; Wang et al. 2022; Robertson et al. 2023; Li et al. 2024). In astrophysical image analysis, ML techniques have found widespread applications across diverse scientific tasks, including galaxy morphology classification (e.g., Banerji et al. 2010; Kim & Brunner 2017; Walmsley et al. 2023a; Vavilova et al. 2021), detection of rare astronomical phenomena such as galaxy mergers, strong gravitational lensing systems, and ultra-diffuse galaxies (e.g., Li et al. 2020; Omori et al. 2023; Stein et al. 2022; Keerthi-Vasan et al. 2023; Thuruthipilly et al. 2025), artifact detection and removal (e.g., Zhang & Bloom 2020; Xu et al. 2023; Tanoglidis

et al. 2022; Zhang & Brandt 2021), and image restoration through super-resolution and denoising (e.g., Sweere et al. 2022; Dabbech et al. 2022; Terris et al. 2023; Vavilova et al. 2021; Liu et al. 2025).

The development of ongoing and future wide-field imaging surveys such as Euclid (Euclid Collaboration et al. 2022), Large Synoptic Survey Telescope (LSST, Ivezić et al. 2019), James Webb Space Telescope (JWST, Gardner et al. 2023; Casey et al. 2023; Bezanson et al. 2024; Finkelstein et al. 2025), will further necessitate the demands for ML-based image analysis.

Despite the growing requirements for ML in astronomical imaging analysis, the generalization of ML models to large-scale surveys remains a challenge (e.g., Sun et al. 2023b; Pearce-Casey et al. 2024). The performance of ML models is often limited by the representative-

ness and quality of the training data, which are usually from simulations or human annotations (e.g., Hart et al. 2016; Hausen & Robertson 2020; Villaescusa-Navarro et al. 2021; Wang et al. 2022; Ono et al. 2024). Numerical simulations may not be able to generate realistic mock data due to limited understanding of underlying physical processes and possible instrumental systematics (e.g., Pearce-Casey et al. 2024), while human-annotated datasets are relatively expensive to obtain and are always biased towards bright and common type objects (e.g., Hart et al. 2016; Speagle et al. 2019a; Sun et al. 2023b,a). All such limitations can lead to poor generalization of ML models to real research environments, especially for those rare but scientifically valuable objects.

To increase the generalizability of ML models in research environments, various attempts have been made. For example, unsupervised/self-supervised learning (e.g., Bishop 2006; Goodfellow et al. 2016; Gui et al. 2023) leverages unlabeled data to learn useful representations without the need for extensive labeled datasets. This approach has been applied in astronomy to improve the performance of models on tasks such as galaxy morphology classification and anomaly detection (e.g., Hayat et al. 2021; Wei et al. 2022; Walmsley et al. 2022; Desmons et al. 2024; Mohale & Lochner 2024; Riggi et al. 2024) and further inspired the recent development of astronomical foundational models (e.g., Walmsley et al. 2022; Sun et al. 2023b; Leung & Bovy 2024; Walmsley et al. 2024).

Semi-supervised learning (e.g., van Engelen & Hoos 2020; Yang et al. 2021) combines a small amount of labeled data with a large amount of unlabeled data during training, which has been shown to enhance model performance in scenarios where labeled data is scarce (e.g., Ćiprijanović et al. 2023; Slijepcevic et al. 2022). Transfer learning (e.g., Zhuang et al. 2019) uses pre-trained models from related domains and performs domain adaptation for specific tasks for deployments, boosting astrophysical ML model deployments in real-world research (e.g., Kim et al. 2021; O’Brian et al. 2021; Cavuoti et al. 2024).

Active learning (e.g., Zhan et al. 2022) iteratively selects the most informative samples for labeling, thereby reducing the labeling effort while maximizing model performance, which has been employed to label rare objects in astronomy (e.g., Leoni et al. 2022; Pruzhinskaya et al. 2023; Andersson et al. 2024). Reinforcement learning (Sutton & Barto 2018) learns from self-play experiences guided by scientific rewards, and while underutilized in astronomy, shows promise for agent-based discovery in astrophysical ML development (e.g., Tenachi et al. 2023; Sun et al. 2024b).

While the methodologies mentioned above approach the challenge of data scarcity from different angles, recent

advancements in deep generative models, particularly diffusion-based models for image and video generation (e.g., Dhariwal & Nichol 2021; Rombach et al. 2021; Ho et al. 2022; Gupta et al. 2023; Ma et al. 2025), open new possibilities for addressing this issue. Today’s generative models not only produce high-quality, realistic images but also enable generative extrapolation into unseen domain. For instance, in the automotive industry, diffusion models can simulate various driving scenarios that may rarely occur in real-world data, such as extreme weather conditions, vehicle malfunctions, or unexpected pedestrian behaviors (e.g., Gao et al. 2024; NVIDIA et al. 2025).

By extrapolating on those rare scenarios, manufacturers can train autonomous driving systems more comprehensively, improving their ability to handle rare and critical situations, thus enhancing safety and reducing the costs associated with extensive real-world testing. As a result, research outside astronomy has begun to explore these models as potential world simulator to reduce the costs associated with robotic training, autonomous driving, and computer vision tasks (e.g., Zhu et al. 2023; Azizi et al. 2023; Song et al. 2023).

This progress has also paved the way for a series of studies exploring the use of diffusion models to generate galaxy images, each tailored to distinct scientific applications (e.g., Smith et al. 2022; Lizarraga et al. 2024; Vičánek Martínez et al. 2024; Sether et al. 2024; Campagne 2025). Building on these achievements, we seek to address the generalization challenge in astronomical image analysis by employing a conditional diffusion model as a realistic galaxy image simulator for data augmentation.

In this study, we demonstrate the capabilities of our generative model, which is trained on Galaxy Zoo 2, one of the largest citizen science galaxy morphological dataset to date. Our generative model could learn and generate diverse, high-fidelity galaxy images that accurately capture the visual characteristics of real astronomical objects and adhere closely to specified morphological conditions. By integrating these synthetic images into machine learning workflows, we observe substantial enhancements in model performance within real-world astronomical research contexts, especially for the analysis of rare and scientifically interesting celestial objects.

We validate our approach through two key tasks: classical galaxy morphology classification and rare object detection. In the realm of classical morphology classification, which encompasses a series of binary classification tasks such as differentiating early- from late-type galaxies and determining the presence of bulge/disk/bar, our model achieves up to a 30% improvement in both

completeness and purity metrics. For the rare object detection task, we focus on identifying early-type galaxies with prominent dust lane features. Given that previous studies (Kaviraj et al. 2012; Shabala et al. 2012; Davis et al. 2015) have simply identified 352 positive samples (approximately 0.1% of the GZ2 dataset), our approach leveraging those synthetic early-type dust-lane galaxies successfully uncovers an additional 520 positive samples that were overlooked due to the limitations of visual inspection in archival data.

This work demonstrates the potential of generative models as surrogates to address data scarcity in astronomy, enhancing machine learning applications for large-scale surveys and promoting the development of astrophysical image foundation models. The paper is structured as follows: Section 2 details the diffusion model, training, and inference; Section 3 describes the Galaxy Zoo 2 dataset and data preprocessing; Section 4 shows the model’s ability to generate high-fidelity galaxy images matching specified morphological features and presents its applications in classical galaxy morphology classification and the detection of rare early-type galaxies with dust lanes (about 0.1% of the dataset). Section 5 explores broader scientific applications beyond galaxy morphology and synergies with other algorithms before concluding.

All models, data, and code used in this study are publicly accessible in <https://github.com/chenruiRae/GalaxySD>. All machine learning models in this study are trained in one NVIDIA GeForce RTX 3090 Graph Processing Unit. Where necessary, we assume parameters for the flat  $\Lambda$ CDM cosmology determined by the Planck Collaboration et al. (2020) (i.e.,  $h = 0.674$ ,  $\Omega_m = 0.315$ ).

## 2. METHOD

Diffusion models (e.g., Ho et al. 2020; Song et al. 2020) are a class of generative models that have shown great promise in generating high-quality images. The core idea behind diffusion models is to model the data distribution by gradually transforming a simple distribution, such as Gaussian noise, into the target data distribution through a series of diffusion steps. This process can be thought of as a reverse diffusion process, where noise is progressively removed to generate realistic samples. Their ability to generate high-quality images with fine details and diverse features makes diffusion models well-suited for various astronomical downstream tasks (e.g., Zhao et al. 2023; Rouhiainen et al. 2024; Vičánek Martínez et al. 2024; Smith et al. 2022; Lizarraga et al. 2024; Vičánek Martínez et al. 2024; Sether et al. 2024).

Mathematically, given an input galaxy image  $\mathbf{x}_0$  with corresponding morphological condition  $\mathbf{c}$  (see Table 1

for examples), a conditional diffusion model tries to extend model the probability distribution  $p(\mathbf{x}_0|\mathbf{c})$  by iteratively denoising a normally distributed variable  $\mathbf{x}_T$ , which can be viewed as modeling a reverse process of a Markov Chain  $\mathbf{x}_T, \mathbf{x}_{T-1}, \dots, \mathbf{x}_0$ . The reverse process is parameterized by a neural network with parameters  $\theta$  and aims to predict a denoised variant  $\epsilon_\theta(\mathbf{x}_t, \mathbf{c})$  from their input  $\mathbf{x}_t$ , where  $\mathbf{x}_t$  is a noisy version of input  $\mathbf{x}_0$ . The training objective can be simplified as regressing the noise at each time step:  $\text{loss} = \mathbb{E}_{\mathbf{x}_t, \epsilon \sim \mathcal{N}(0, \mathbf{I}), t} \|\epsilon - \epsilon_\theta(\mathbf{x}_t, \mathbf{c})\|^2$ .

In practical implementation, we utilize the pre-trained diffusion model **Stable-Diffusion-v1.5**<sup>1</sup> (Rombach et al. 2021). This model adopts a U-Net architecture (Ronneberger et al. 2015) combined with a text encoder. Input morphological conditions are first vectorized by the text encoder, then integrated into the image generation process via a cross-attention mechanism, detailed in Appendix C. These design features enable efficient and flexible processing of conditional inputs. We fine-tune the entire model using morphology condition-galaxy image pairs extracted from the GZ2 datasets (see Section 3 for details). Through full-parameter fine-tuning, the model adapts to the unique characteristics of astronomical imagery, enabling it to generate realistic, high-fidelity galaxy images that accurately capture subtle morphological details.

We have observed that images generated solely with text conditioning consistently display a pattern of systematic over-brightness. This phenomenon stems from the singularities present in the diffusion process at the  $t = 1$  timestep, as documented in previous works (e.g., Lin et al. 2023a; Zhang et al. 2024). To address this issue, we incorporated randomly selected reference images and initiated the denoising process from the noised reference image. This strategic modification serves to effectively regulate the brightness levels of the generated images while preserving their visual fidelity.

When performing generative extrapolation on unseen classes—specifically early-type galaxies with prominent dust lanes in this study, we observe that underrepresented features (e.g., dust lanes) can be diluted to varying degrees, depending on their prevalence in the training data. To address this, we implement a targeted feature enhancement strategy during inference. After converting input morphological prompts or descriptions into contextual embeddings, we scale the weights of the target features (e.g., dust lanes) to bias the cross-attention mechanism toward prioritizing these attributes. This weighting scheme enables the model to focus more in-

<sup>1</sup> <https://huggingface.co/stable-diffusion-v1-5/stable-diffusion-v1-5>

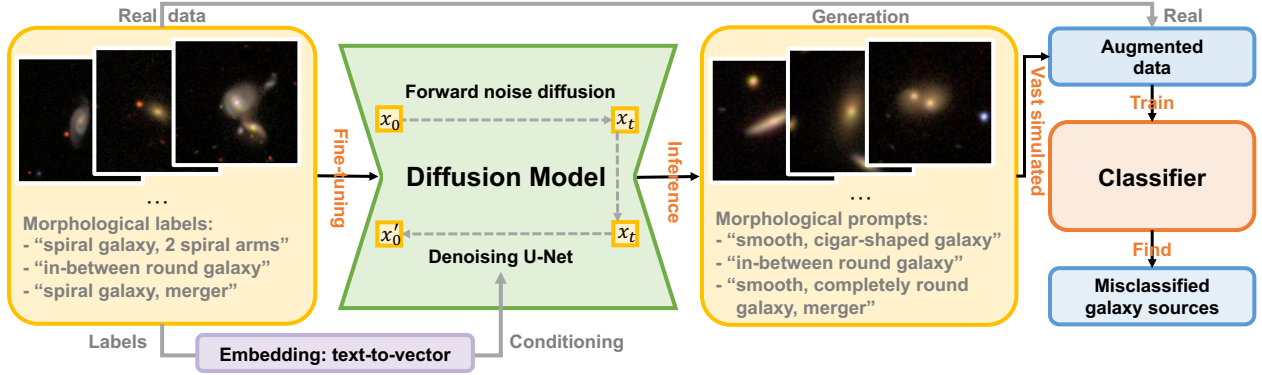


**Figure 1.** Schematic diagram of our diffusion model and its applications to downstream tasks. For the training processes shown in the left two boxes, the training set consists of real images and descriptive morphological prompts (see Table 1 for more examples) from Galaxy Zoo 2, which are used to fine-tuning diffusion model. For inference, given morphological prompts, our fine-tuned model generates realistic and diverse galaxy images as demanded. These vast simulated galaxy images integrate with real data could be a high-quality augmented dataset used for other downstream ML tasks as detailed in Section 4.

tentionally on underrepresented characteristics, thereby producing synthetic images with enhanced fidelity to the specified features—an approach particularly critical when extrapolating beyond the distribution of the training dataset.

After fully training the conditional generative model, our diffusion model learns the mapping between morphological conditions and corresponding visual features. It can synthesize galaxies from our dataset and extrapolate to rare or even unseen scenarios, for example, imagining an early-type galaxy exhibiting star-forming characteristics. These hypothetical entities, though rare or even never observed, hold scientific value. Incorporating these synthesized images into downstream machine learning model training pipelines can notably improve model performance on ill-defined problems and may lead to potential unique scientific discoveries.

### 3. DATA

In this study, we focus on synthesizing images based on text-formatted morphological features (see Table 1 for example). These visual characteristics are critical in various scientific tasks, including Hubble-sequence galaxy morphology classification and the identification of key physical phenomena such as bar, bulge, strong lensing, tidal features, and dust lanes (e.g., Dalcanton et al. 2004; Kreckel et al. 2013; Morales et al. 2018; Hood et al. 2018; Metcalf et al. 2019; Li et al. 2020).

To achieve this, we used the normal-depth Sloan Digital Sky Survey samples of Galaxy Zoo 2 (hereafter GZ2)<sup>2</sup> debiased by the method described in Hart et al. (2016), which contains 239,695 galaxy images labeled by human

volunteers using a hierarchical morphological classification system (e.g., Lintott et al. 2008; Willett et al. 2013; Hart et al. 2016; Walmsley et al. 2023b). In this section, we describe the Galaxy Zoo 2 dataset, outline the preprocessing steps used to prepare the data for training the diffusion model, and explain the structure employed for galaxy morphology conditions. Despite we here focus on morphological features in this work, our method can be easily extended to other astrophysical properties, such as redshift, stellar or halo mass, dust content and so on, which we give more discussion in Section 5.

#### 3.1. Galaxy Zoo Project

Galaxy Zoo 2 (Willett et al. 2013) has proven invaluable for advancing galaxy morphology studies and facilitating the development of machine learning approaches in astrophysics. It serves as an ideal test bed for our methodology by providing a labeling system (see Appendix B for details), encompasses not only standard Hubble-Sequence classifications but also detailed morphological distinctions, such as mergers, spiral structure, tidal features, and more. This hierarchical classification enables the generation of images conditioned on specific morphological features, which is crucial for data augmentation in various astronomical applications, including galaxy morphology study, rare object identification, and verification of observational data pipelines.

As a citizen science project, Galaxy Zoo 2 benefits from volunteer contributes but such treatment also introduces noise. We here propriety training set quality before data size to ensure better performance of our generative model.

To achieve that, we follow the subsample procedure presented in Willett et al. (2013), through which galaxies could be considered whether well sampled or not based

<sup>2</sup> <https://data.galaxyzoo.org>



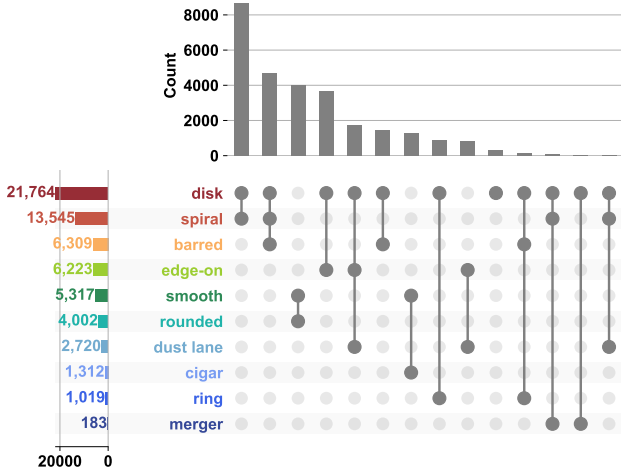


**Figure 2.** Upset plot to visualize the morphology distribution in our training samples. The gray dots and connections represents co-occurrence of different morphological features in the dataset. Bars indicate the counts of individual features and their combinations. We simply show primary tag categories, excluding detailed tags such as bulge prominence, the number of spiral arms, etc. This highly imbalanced distributions emphasize the necessity of incorporating synthetic data for robust machine learning training.

on three determined criteria. Firstly, the vote fraction for a given task must exceed thresholds related to preceding tasks (see Table 3 in Willett et al. (2013) for details), ensuring the question is sufficiently well-answered. Then, the number of votes must be greater than 20, to reduce variability caused by limited sample sizes. Last, the debiased vote fraction must exceed 0.8 to free from significant biases. The debiased vote fraction is an adjusted vote fraction for classification bias like small, faint and weird galaxy cases, which can be obtained from GZ2 data straightforwardly. For example, to identify whether a galaxy is a disk viewed edge-on, select vote fraction  $p_{\text{features}/\text{disk}} > 0.430$  as per the table mentioned earlier,  $N_{\text{edge-on}} > 20$ , and debiased vote fraction  $p'_{\text{edge-on}} > 0.8$ . Such treatment lead to 71,455 galaxies with relatively high confidence morphology labels.

However, this sample is highly imbalanced, while some morphologies appear much more frequently than others. To mitigate this imbalance and avoid the model biased toward the more frequent labels, we down-sample those overrepresented labels to 2,000 to better align with the occurrence of rarer tags. Such treatment can avoid overfitting and improve generalizability. For example, 14,835 galaxy images labeled as “smooth, completely round galaxy” are randomly sampled to 2,000.

Additionally, non-informative or scientifically irrelevant tags (e.g., “star or artifact”, “something odd”) are removed to concentrate the learning process on mean-

ingful morphological features. Finally, to facilitate the diffusion model’s ability to learn specific visual attributes, we randomly sample and shuffle the tags during training. This approach ensures that the final dataset is balanced, consistent, and diverse, providing an effective foundation for subsequent model training.

We use the pseudo-colored images from the GZ2 dataset as model inputs because they could clearly reflect the morphologies across various broad bands—a common practice in similar studies (e.g., Willett et al. 2013, 2017; Walmsley et al. 2023b). Our labeling pipeline begins by converting the raw probabilistic classification results from the GZ2 catalog into text-formatted labels that precisely adhere to the GZ2 classification standards. Each galaxy image is assigned a set of labels by traversing a branched flowchart of questions as shown in Figure B3. We present examples in Table 1. Finally, 27,910 annotated galaxy images are used to fine-tuning diffusion model. The distribution of the tags can be roughly seen in the right histogram of Figure 2.

### 3.2. Early-type Dust Lane Galaxy Catalog

In addition to the GZ2 galaxy morphology catalog, we also incorporate a catalog of early-type galaxies (ETGs) with prominent dust lanes from Kaviraj et al. (2012) to demonstrate our generative model’s capability to synthesize rare objects by extrapolating from common visual features and by enhancing downstream ML training pipelines.

Although early-type galaxies and dust lanes are individually common, their combination—“dusty” early-type galaxies (hereafter, D-ETGs) are rare, serving as a tracer of minor merger events and offering valuable insights into galaxy evolution. To date, Kaviraj et al. (2012) presents one of the largest D-ETG catalogs, containing 352 nearby D-ETGs ( $0.01 < z < 0.1$ ) identified from approximately 300,000 galaxies in the GZ2 dataset. This catalog was constructed by first selecting galaxies with at least one volunteer marking the presence of a dust lane, which produced 19,000 galaxy candidates, and subsequently having these candidates visually inspected by expert astronomers to confirm both the presence of a dust lane and the galaxy’s early-type morphology.

We construct our rare object detection task by using this 352 D-ETGs as positive samples and demonstrate that our generative model can effectively generate synthetic D-ETGs to augment the training set and improve the performance of ML models in identifying these rare objects in Section 4.3. We excluded those 352 D-ETGs, as well as galaxies labeled as combination of early-type features (e.g., completely round or in-between round) and dust lane feature, when training our diffusion mod-

els. This exclusion was made to prevent potential data leakage and to highlight the capability of generative models in performing generative extrapolation on rare morphological structures.

#### 4. RESULT

In this study, we address the data scarcity challenges in large-scale galaxy image analysis by leveraging diffusion models for data augmentation. We begin by evaluating the quality of the generated images and then demonstrate the effectiveness of the synthetic images in enhancing the performance of machine learning models across various scientific applications. These include general galaxy morphology classification and a rare object detection task focused on early-type galaxies with prominent dust-lane features, thereby underscoring the practical value of our methodology in real-world research environments.

Type	Prompt
A	cigar-shaped galaxy
B	completely round galaxy
C	edge-on galaxy
D	in-between round galaxy
E	ring galaxy
F	spiral galaxy with 4 spiral arms
G	spiral galaxy with loosely wound 2 spiral arms
H	spiral galaxy with tightly wound spiral arms
I	spiral galaxy with just noticeable central bulge prominence
J	spiral galaxy with obvious central bulge prominence
K	in-between round galaxy, {dust lane:1.3}
L	edge-on galaxy, {dust lane:1.3}, with rounded edge-on bulge
M	bar-shaped structure in the center of galaxy
N	edge-on galaxy, with rounded edge-on bulge
O	in-between round galaxy, merger
P	spiral galaxy, just noticeable bulge prominence, merger

**Table 1.** Morphological conditions employed in generating the diverse galaxy images in Figure 3. In K and L prompts, {dust lane:1.3} assigns a 1.3× weight to the dust lane feature during inference through cross-attention mechanism, emphasizing its prominence. See Appendix B for the detailed hierarchical morphology classification system.

##### 4.1. Generated Image Quality Evaluation

In this study, we focus on the visual features of galaxy images. Accordingly, we evaluate the quality of the generated images—assessing realism, diversity, and consis-

tency—using computer vision-based metrics (e.g., Astolfi et al. 2024) rather than traditional astrophysical metrics (e.g., flux (e.g., Smith et al. 2022; Vičánek Martínez et al. 2024), radius and ellipticity (Lanusse et al. 2021), standard CAS statistics (Conselice et al. 2000; Conselice 2003), as well as the Gini coefficient and M20 statistics (Lotz et al. 2004)).

Although these astrophysical metrics are closely related to the physical properties of galaxies, they are not well suited for our study for two reasons: (1) they may not capture the diverse and intricate visual details—such as spiral arms, mergers, dust lanes, lenses, or arcs—present in galaxy images, and (2) they cannot be directly applied to the pseudo-colored images used in our analysis. We also note here that there lacks unified evaluation system for synthesized or simulated galaxy images (e.g., Smith et al. 2022; Hackstein et al. 2023; Vičánek Martínez et al. 2024), and the metrics we use here pose new direction for future work.

Our evaluation framework assessed three critical aspects of generated galaxy images: (1) realism (visual fidelity relative to real observations), (2) diversity (morphological variety across outputs), and (3) consistency (adherence to input conditions). Formally, let the real image dataset be  $\mathbf{X} = \{X_i \mid i = 1, \dots, N', X_i \in \mathbb{R}^{H \times W \times 3}\}$  and the synthesized dataset be  $\mathbf{Y} = \{Y_j \mid j = 1, \dots, N, Y_j \in \mathbb{R}^{H \times W \times 3}\}$ . For a visual condition  $p$  (e.g., GZ2-annotated features; see Section 3), conditional realism  $\mathcal{R}_C^p$  is quantified as below:

$$\mathcal{R}_C^p = \frac{1}{N} \sum_{j=1}^N \max_i (\mathcal{S}(f_\phi(X_i), f_\phi(Y_j))), \quad i \in \{1, \dots, N'\}, \quad (1)$$

where  $f_\phi(\cdot) : \mathbb{R}^{H \times W \times 3} \rightarrow \mathbb{R}^n$  is a SimCLR-based encoder (Chen et al. 2020) mapping images to an  $n$ -dimensional embedding space (implementation details in Appendix A), and  $\mathcal{S}$  denotes cosine similarity. The global realism  $\mathcal{R}$  averages  $\mathcal{R}_C^p$  across all conditions  $p \in \mathbf{P}$ :

$$\mathcal{R} = \frac{1}{|\mathbf{P}|} \sum_{p \in \mathbf{P}} \mathcal{R}_C^p. \quad (2)$$

The conditional diversity  $\mathcal{D}_C^p$  is defined as:

$$\mathcal{D}_C^p = \frac{1}{N \cdot N'} \sum_{i=1}^{N'} \sum_{j=1}^N \mathcal{S}(f_\phi(X_i), f_\phi(Y_j)), \quad (3)$$

measuring average similarity between real and synthesized image pairs under condition  $p$ . The overall diversity  $\mathcal{D}$  is computed analogously to realism:

$$\mathcal{D} = \frac{1}{|\mathbf{P}|} \sum_{p \in \mathbf{P}} \mathcal{D}_C^p. \quad (4)$$

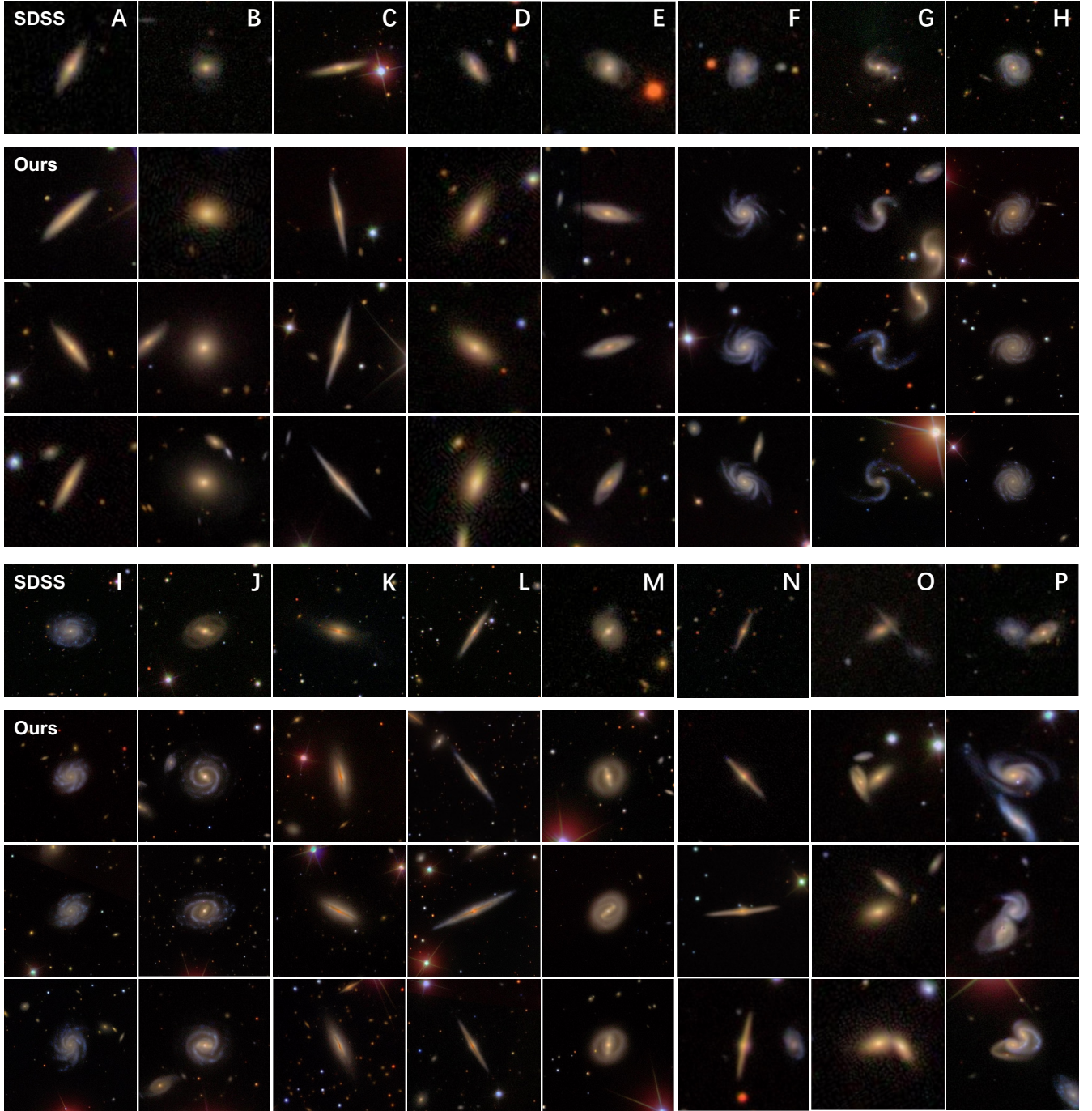


**Figure 3.** Comparison of galaxy images generated by our model under various morphology-related text prompts, compared with real galaxy images. For each column annotated by a capital letter in top-right corner, the leading first image is a real one from SDSS, while the following three images are synthesized by our model. The annotated capital letters represents prompts used to generate simulated galaxies as Table 1 shows.



It’s worth noting that the diversity metric measures how similar two images are when generated from the same morphology condition. As such, the smaller the diversity value, the greater the variety between the images.

To evaluate the conditional consistency  $\mathcal{C}^p$ , we use the commonly adopted visual question answering (VQA) approaches (e.g., Hu et al. 2023; Cho et al. 2023; Astolfi et al. 2024). In detail, we train a series binary classifier  $\mathbf{Q}_i$  tailored to different visual features, such as, the presence of spiral arm, if this is a ring on galaxy, etc. The conditional consistency  $\mathcal{C}^p$  is then defined as the average accuracy of the classifiers  $\mathbf{Q}_i$  under condition  $p$ :

$$\mathcal{C}^p = \frac{1}{N} \sum_{j=1}^N \frac{1}{Q_j} \sum_{i=1}^{Q_j} \mathbb{I}(\mathbf{Q}_i(Y_j) = A_i) \quad (5)$$

where  $Q_j$  represents the number of binary classifiers employed for image  $Y_j$  (11 in this work),  $A_i$  is the ground truth to classifier  $\mathbf{Q}_i$  on image  $Y_j$ , and  $\mathbb{I}(\cdot)$  is the indicator function. The global consistency  $\mathcal{C}$  is the average of  $\mathcal{C}^p$  across all conditions  $p \in \mathbf{P}$ :

$$\mathcal{C} = \frac{1}{|\mathbf{P}|} \sum_{p \in \mathbf{P}} \mathcal{C}^p. \quad (6)$$

Above metrics were tracked throughout the training iterations to monitor progressive improvements in image quality. As shown in Figure 4, the realism of the generated images rapidly improve during the first 1,000 steps before continuing to grow steadily. Examples in Figure 3 illustrates that our synthesized images closely resemble real galaxy images by capturing a wide range of morphological features—including spiral arms, dust lanes, and signs of mergers—according to the given conditions. Furthermore, Figure 4 reinforces that the diversity of the generated images increases continuously, demonstrating the model’s gradual mastery of detailed galaxy morphology, which is also evident in Figure 3.

We also notice that there is Pareto front between the realism and diversity of the generated images, as shown in Figure 5. This indicates that while our model can generate images with high realism, it may sacrifice some diversity in the process. This trade-off is common in generative models, where achieving high realism often leads to less diverse outputs. However, we find that our model maintains a good balance between these two aspects, producing images that are both realistic and diverse.

Overall, our diffusion model successfully generates high-quality galaxy images that closely resemble real observations. The model exhibits strong realism, diversity, and consistency, as evidenced by the visual fidelity, morphological variety, and adherence to input conditions

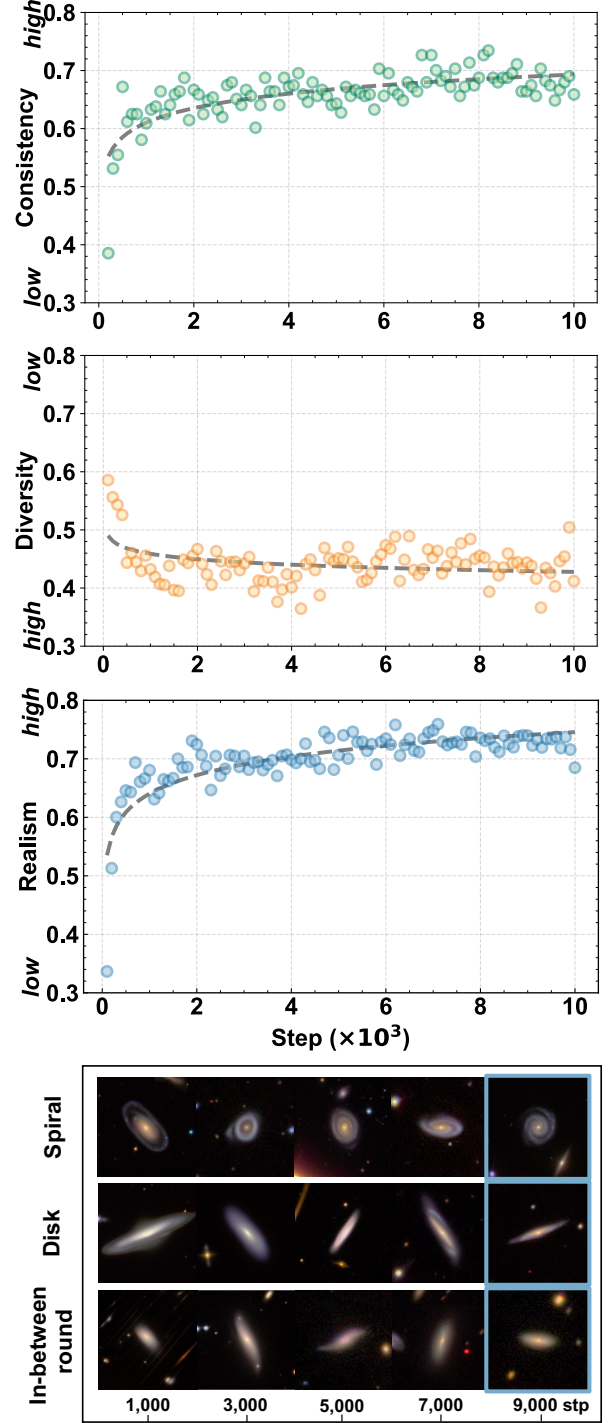


**Figure 4.** The quantified consistency, diversity and realism of generated galaxy images with training steps increasing, under average prompts. The lower panel intuitively demonstrates that under various prompts, the more training steps evolve, the more real generated galaxy images are.



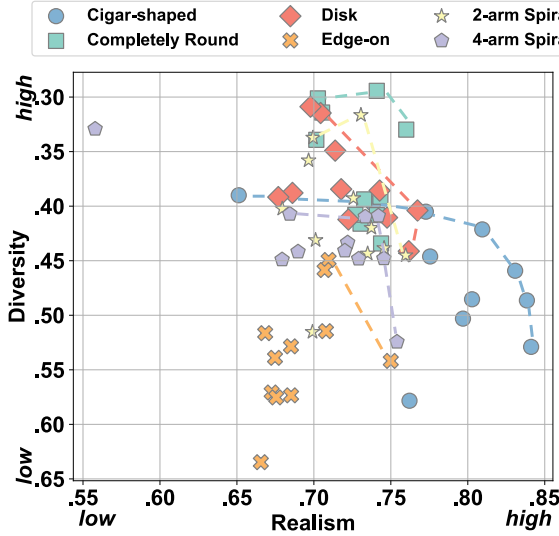


**Figure 5.** Pareto fronts showing the trade-off relationship between realism and diversity evaluation indicators of our diffusion model. The dashed lines are Pareto fronts representing the frontiers of optimal solutions to the three evaluation metrics. Different colors represent different types of morphological prompts as top legend shows.

of the generated images. These results underscore the potential of our approach to enhance machine learning performance in various scientific applications, as detailed in the following sections.

#### 4.2. Improving Galaxy Morphology Classification with Synthetic Data

As we have demonstrated that our diffusion model can generate high-fidelity galaxy images, we now show how these images can bring tangible scientific benefits. We first focus on classical binary classification tasks involving key galaxy morphologies, including spirals, edge-on disks, bars, and bulges. These features are critical for understanding various astrophysical processes, such as the role of spiral arms in star formation (e.g., Foyle et al. 2010; Schinnerer et al. 2017; Sun et al. 2024a), the close relationship between presence frequency of disk galaxies with  $\Lambda$ CDM cosmology (e.g., Neeleman et al. 2020; Nelson et al. 2023; Yan et al. 2024; Kohandel et al. 2024), the influence of bars on gas inflow and central starbursts (e.g., Friedli et al. 1994; Fraser-McKelvie et al. 2019; Lin et al. 2020; Chen et al. 2023), and the prominence of bulges in deciphering galaxy merger histories (e.g., Hopkins et al. 2010; Fontanot et al. 2011; Nedkova et al. 2024).

Despite these types of galaxies being relatively common in the Universe and having been widely studied over the past thirty years, their detailed physical scenarios remain a subject of debate. Accurately identifying them among billions of galaxies is of great scientific value. It not only

	Tasks	Purity	Completeness	F1-Score
Spiral (0.43)	Baseline	0.67	0.45	0.54
	Focal loss	0.65	0.36	0.46
	Ours	<b>0.69</b>	<b>0.70</b>	<b>0.70</b>
Disk (0.09)	Baseline	0.81	0.52	0.63
	Focal loss	0.80	0.76	0.78
	Ours	<b>0.83</b>	<b>0.77</b>	<b>0.80</b>
Bar (0.10)	Baseline	0.59	<b>0.95</b>	0.73
	Focal loss	0.61	0.85	0.71
	Ours	<b>0.67</b>	0.86	<b>0.75</b>
Bulge (0.07)	Baseline	0.30	0.57	0.40
	Focal loss	0.30	0.72	0.42
	Ours	<b>0.32</b>	<b>0.75</b>	<b>0.44</b>

**Table 2.** Performance comparison across classical binary classification tasks. The annotated fractions represent the proportion of positive samples in the full dataset. We focus on metrics for positive samples only, as negative sample metrics are uniformly high and do not effectively highlight differences between methods. Notably, machine learning models trained on our augmented dataset consistently outperform both baseline models and those using adjusted metrics.

helps us understand their formation mechanisms but also provides insights into cosmology (e.g., Haslbauer et al. 2022; Wittenburg et al. 2023; Hopkins et al. 2023).

While these morphological features are much common compared to those rare-events such as strong lensing, tidal features, and dust lanes, they are still challenging to identify due to the lack of high-quality labeled datasets and the inherent class imbalance. As our generative model can produce a large number of realistic galaxy images with specific morphological features, we can use these synthetic images to enhance the training set for machine learning models.

In this experiment, we split the GZ2 dataset into a training set (90%) and a test set (10%). Specifically, we further randomly select 10% of the training data to form a validation set. For each task, we fix the number of negative samples at 10,000 and sample positive samples proportionally to maintain the same class distributions as the GZ2 full dataset (containing 239,695 galaxies). For the four selected morphological features, they have different difficulties in classification due to their different positive sample fractions and contamination rates from volunteer annotations. We here neglect the possible contaminations in the training set, as the contamination rate should not dominate the final results since we take a relative conservative data selection criteria as described in Section 3.

The positive fractions of the four features, as annotated by volunteers, are 0.43, 0.09, 0.10, and 0.07 for spiral, disk, bar, and bulge features, respectively. We then use the GZ2 dataset to train a convolutional neural network (CNN) model with a ResNet-18 backbone (He et al. 2016) for each of the four morphological features. The model is trained using a binary cross-entropy loss function and an Adam optimizer with a learning rate of  $10^{-4}$ . We also apply standard data augmentation such as random cropping, rotation, and flipping to improve the model’s generalization ability.

To evaluate the performance of our model, we use three metrics: purity, completeness, and F1-score. Purity measures the proportion of correctly classified positive samples among all samples predicted as positive, while completeness measures the proportion of correctly classified positive samples among all actual positive samples. The F1-score is the harmonic mean of purity and completeness, providing a balanced measure of the model’s performance. We compare our model’s performance with two baselines: (1) a pure supervised learning model trained only on the GZ2 dataset and (2) a model trained with focal loss (Lin et al. 2017) to address class imbalance.

The results are presented in Table 2. Our model outperforms both baselines across all four classification tasks, achieving the highest values for purity, completeness, and F1-score. For instance, in the spiral feature classification task, our model attains a purity of 0.69, completeness of 0.70, and F1-score of 0.70—surpassing the baseline model (0.67, 0.45, 0.54) and the focal loss model (0.65, 0.36, 0.46). Similar improvements are observed in the other three tasks. These findings demonstrate that our generative model effectively enhances the performance of machine learning models in identifying key morphological features within galaxy images, particularly for common galaxy morphology classification tasks.

The success of our model stems from the high quality and diversity of the generated images, which provide a rich source of synthetic data for training downstream ML models. Since image generation is a more complex task than binary classification, generative models are less prone to overfitting on systematic biases in the data. This enables them to improve the generalizability of downstream ML models. In astrophysics, data distributions are intrinsically imbalanced due to physical processes governing cosmic evolution. However, robust ML models require large training datasets to avoid becoming trapped in local minima. Our method bridges this critical gap by generating synthetic data to address such imbalances.

	Purity	Completeness	F1-Score
Baseline	0.43	0.43	0.43
Focal loss	0.48	0.16	0.24
Ours	<b>0.74</b>	<b>0.60</b>	<b>0.66</b>

**Table 3.** Performance comparison on the D-ETG identification task. We follow the same experimental setting as in Table 3. The synthesized D-ETG images can substantially enhance the downstream tasks as shown here.

#### 4.3. Enhancing Early-type Dust Lane Galaxy Detection via Extrapolation on Rare Morphologies

As we have demonstrated that our generative model can generate galaxies with common morphologies, we now turn our attention to a more challenging task: identifying early-type galaxies with dust lanes (D-ETGs) by extrapolation on rare morphologies. The rarity of D-ETGs in the universe makes them difficult to be filtered out from large galaxy surveys. For instance, in the work of Kaviraj et al. (2012), around 19,000 galaxies from GZ2 catalog was initially flagged by at least one user as having a dust lane. However, after visual inspection by two experts, only 352 galaxies were verified as D - ETGs. Such low detection rate poses a challenge for machine learning models, as they often struggle to learn from such limited data.

To address this issue, we leverage our generative model to synthesize additional D-ETG images, thereby augmenting the training set and improving the performance of machine learning models in identifying these rare objects. This task is difficult compared to the previous one, as the model needs to learn to extrapolate from common morphological features – early-type features and dust lane features – to extrapolate to the rare D-ETG morphology as shown in Figure 6.

We initiate our investigation with an experimental test. Using the D-ETG catalog from Kaviraj et al. (2012), we aim to verify the effectiveness of our pipeline. In the experimental setup, we randomly select 100 galaxies from the D-ETG catalog in Kaviraj et al. (2012) and 10,000 galaxies from the GZ2 dataset to construct the training set, composing a experimental dataset with 1/100 postive/negative sample ratios, mimic the data distribution in Kaviraj et al. (2012). Similar to the approach in Section 4.2, we use pure supervised learning without any additional adjustments as our baseline.

Again, we introduce Focal Loss as an alternative baseline for dealing with imbalance classes as in Section 4.2. This method reweights the contributions of positive and negative samples in the loss function. We note that we defer detailed comparisons with more advanced few - shot

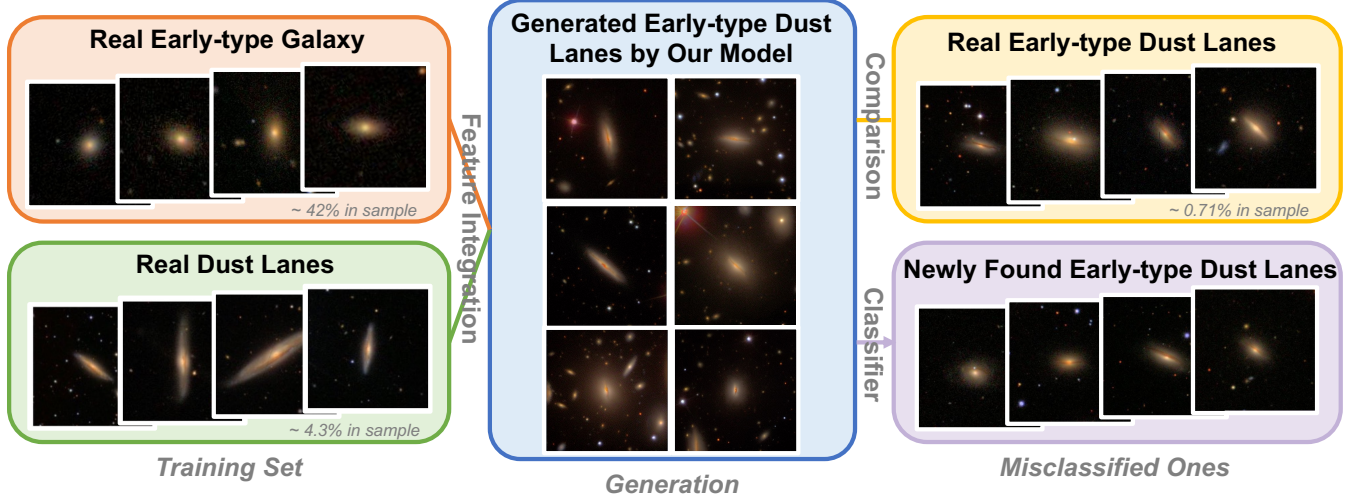


**Figure 6.** Generative extrapolation of early-type galaxies with prominent dust lanes (D-ETGs). While early-type galaxies are commonly quiescent, our generative model synthesizes D-ETGs by merging the morphology feature in early-type galaxy and star-forming feature (dust lane) in late-type galaxies. Both early-type galaxies and dust lanes are common in the universe, but early-type galaxies with dust lanes are rare since they are origin from recent merging events. Our model learns these two concepts from extensive datasets and extrapolates them to synthesize rare D-ETGs. These synthesized D-ETG images are then used as training data for classifiers, facilitating the identification of 520 D-ETGs within a sample of 239,695 GZ2 images as shown in Figure 7.

algorithms and unsupervised classification algorithms to future studies, as their inclusion is beyond the scope of this work. More importantly, our methodologies are not in competition with these algorithms but can be used together to enhance these algorithms through data augmentation, a topic that we will discuss further in Section 5.

Despite the fact that the combination of early - type galaxy and dust lane features is rare in the universe, their individual components (early type galaxies, and galaxies with dust lane) can be easily found and are well - annotated in the GZ2 catalog. Our generative model learns these two dominant features and then extrapolates this concept to the context of early - type dust - lane galaxies. The synthesized D - ETGs, which are presented in Figure 7, mimic realistic D - ETGs and can be generated easily.

As shown in Table 3, injecting our synthesized images into the training pipeline improves the purity from 43% to 74% and the completeness from 43% to 60% at a positive sample ratio of 1/100. Focal Loss, while increasing the purity by 5% by assigning more model weights to rare samples, leads to a decline in completeness, dropping from 43% to 16%. The result demonstrates the potential of our data augmentation based approach in enhancing the performance of galaxy morphology few-shot learning tasks.

Here, we apply our method to 239,695 Galaxy Zoo 2 (GZ2) images to identify previously undetected D-type

early-type galaxies (D-ETGs). We first construct training data: 10,000 synthetic D-ETGs as positive samples and 10,000 randomly selected normal galaxies as negative samples. Given the low occurrence of D-ETGs, we assume minimal contamination in the negative sample set. We follow the training procedure described in Section 4.2. After the initial training, the model was applied to the entire GZ2 dataset, identifying 8,184 positive candidates. These candidates were then visually inspected, and the classifier was retrained based on the validated results, yielding 2,488 refined positive samples. This iterative process was repeated once more, resulting in an additional 1,062 positive samples. All candidate samples in the three iteration training stages were visually validated by three authors (CM, ZS, and TJ). Final selection required agreement from at least two reviewers, resulting in a catalog of 520 high-confidence D-ETGs overlooked in Kaviraj et al. (2012). We also note that a baseline model trained merely on the 352 D-ETGs from Kaviraj et al. (2012) yielded extremely low-purity results, rendering effective detection unfeasible.

These findings align with preliminary experiments in Table 3, highlighting the critical role of synthetic images for enhancing rare object detection. The redshift distribution of our 520 newly identified D-ETGs is shown in Figure 8. Spectroscopic redshift measurements were extracted from the GSWLC catalog (Salim et al. 2016), originating from SDSS spectra (Ahn et al. 2014). As shown, our samples exhibit a broader spread toward



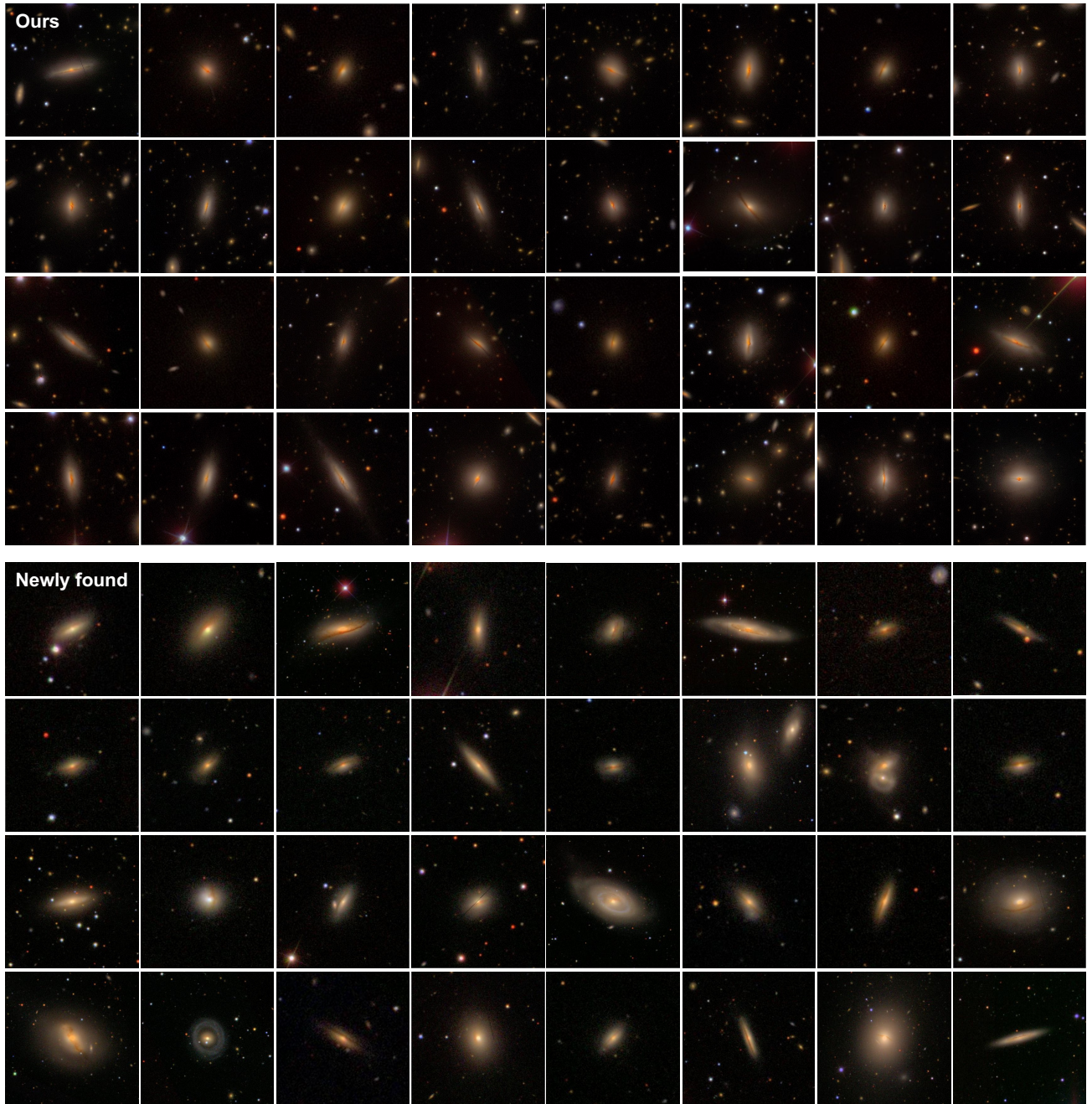


**Figure 7.** Examples of D-ETGs synthesized by our diffusion model (upper panel) and newly identified instances using machine learning models augmented with the synthesized data (lower panel). Our diffusion model generates high-fidelity D-ETG images by prompts like “sdss, {completely round:1.2} galaxy, {dust lane:1.3}” or “sdss, in-between round galaxy, {dust lane:1.3}”, and these synthesized images enhance the efficiency of identifying such objects in real datasets. We manually assign weights to different morphology features through cross-attention mechanism to emphasize generation of desired features as in Section 2.



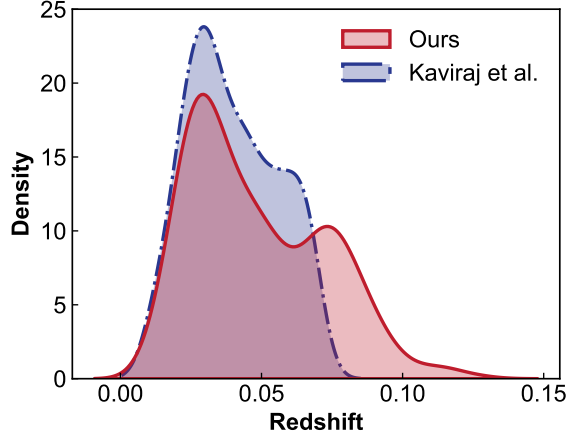


**Figure 8.** Kernel density estimates (KDE) of redshift distributions for D-ETGs identified by our model (red) and Kaviraj et al. (2012) (blue). Redshift values are obtained from the GSWLC (Salim et al. 2016). Our sample encompasses relatively higher redshifts, a regime that is more challenging for human volunteers to identify, thereby demonstrating the efficacy of our synthesized image-enhanced machine learning model in detecting rare galaxy populations.

higher redshifts, making it challenging for humans to laboriously identify them among hundreds of millions of galaxies.

To ensure our sample shares similar physical properties as in Kaviraj et al. (2012), we compare their Star Formation Rate (SFR) and halo mass in Figure 9. The newly found ones were compared with those from Kaviraj et al. (2012) and a control sample of 4000 normal early-type galaxies (ETGs). The control sample was selected to match our sample in redshift and stellar mass distributions (see Appendix D). Stellar mass and SFR measurements are from GSWLC catalogs (Salim et al. 2016), derived via Spectral Energy Distribution (SED) fitting using CIGALE (Noll et al. 2009) with UV and optical photometry (0.15–0.9  $\mu\text{m}$ ). The SED models assumed a two-component exponential star formation history, BC03 stellar populations (Bruzual & Charlot 2003), and Calzetti attenuation law (Calzetti et al. 2000). Halo masses were drawn from group catalogs in Yang et al. (2012). We found that the D-ETGs in this work exhibit higher star formation rates than their normal counterparts, consistent with the samples in Kaviraj et al. (2012). These galaxies are also more likely to reside in field and group environments, suggesting their origin from merger events (Pearson et al. 2024).

Our approach ultimately identifies 520 D - ETGs that were overlooked in Kaviraj et al. (2012), thereby opening up new avenues for understanding merger events and dust properties in nearby galaxies.

## 5. DISCUSSION

Our work demonstrates the potential of diffusion models to generate high-fidelity galaxy images that closely mimic real astronomical observations while enforcing specified morphological characteristics. By integrating these synthetic images into machine learning (ML) training pipelines, we enhance the performance of diverse scientific tasks—from classical morphological classifications (e.g., bars, spirals, disks, bulges) to the more challenging detection of rare objects such as dusty early-type galaxies (D-ETGs). While state-of-the-art hydrodynamical simulations remain computationally intensive and often struggle to resolve fine-scale observational details, our diffusion models can synthesize large datasets of observationally realistic images on a single GPU. These synthetic galaxies facilitate the identification of analogous systems in real astronomical surveys, forming a real-to-synthetic-to-real workflow that provides new observational constraints on those elusive phenomena.

Our methodology is readily adaptable to other galaxy populations of high scientific relevance, such as strong lensing systems (e.g., Brownstein et al. 2012; O’Riordan et al. 2025; Deng et al. 2025), red spirals (e.g., Masters et al. 2010; Fudamoto et al. 2022; Cui et al. 2024), tidal features (e.g., Hood et al. 2018; Khalid et al. 2024; Rutherford et al. 2024), ultra-diffuse galaxies (e.g., Li et al. 2023; Wei et al. 2025; Buzzo et al. 2025) and etc. Detailed implementation for each system lies beyond the scope of this study and will be explored in future investigations. Additionally, for modern large-scale sky surveys, substantial quantities of high-fidelity synthetic data encompassing diverse galaxy types and observational conditions are critical for developing and validating data processing pipelines. Our diffusion model, therefore, can efficiently generate such validation data, thereby contributing to this domain as shown in previous studies (e.g., Rowe et al. 2015; Lanusse et al. 2021). By further integrating instrumental characteristics (e.g., noise level, PSF) and physical properties (e.g., stellar mass, dynamical information), we envision a unified “simulator” that captures complex correlations within multi-dimensional observational datasets.

The implications of our work extend to a broad spectrum of astrophysical research domains. For example: (1) In radio astronomy, projects such as Radio Galaxy Zoo (e.g., Banfield et al. 2015; Tang et al. 2020; Bowles et al. 2023) could leverage our pretrained models to classify intricate radio galaxy morphologies, such as bent jets or diffuse lobes. (2) For near-Earth object (NEO) detection, our framework could generate synthetic NEOs with realistic trajectories and observational systematics to enhance detection algorithms for hazardous asteroids

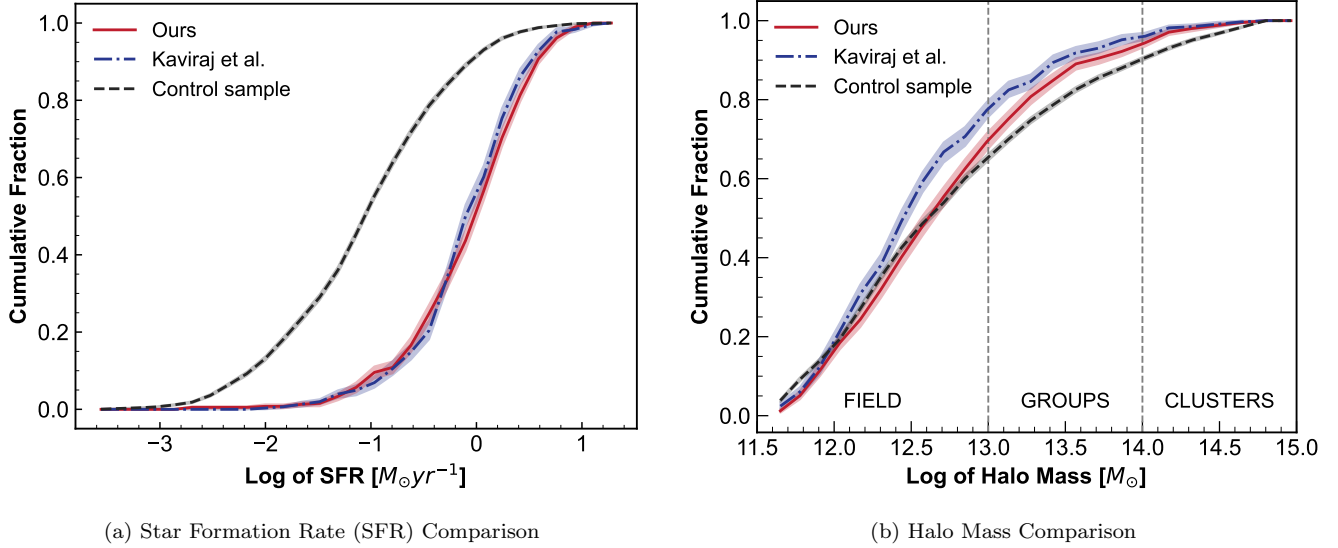


**Figure 9.** Cumulative distributions of star formation rate (SFR; left) and halo mass (right) are shown for our D-ETG dataset, the Kaviraj et al. (2012) sample, and a control ETG sample. SFRs are drawn from the GSWLC catalog (Salim et al. 2016), and halo masses are derived from the group catalog in Yang et al. (2012); shaded regions denote  $1\sigma$  bootstrap errors for the cumulative distribution functions (CDFs). Despite their early-type morphology, our sample exhibits higher SFRs than control ETGs, aligning with Kaviraj et al. (2012) and indicating substantial star-forming activity. These galaxies preferentially inhabit field and group environments (consistent with Kaviraj et al. (2012)), suggesting a history of strong interactions. Together, these results imply their physical origin as minor merger remnants.

(e.g., Duev et al. 2019; Irureta-Goyena et al. 2025). (3) In planetary geology, synthetic surface maps of icy moons could train terrain ML models for upcoming missions (e.g., Bhaskara et al. 2024). The same workflow can also be extended to other data modalities, such as spectra, integral field unit (IFU) data, and others.

Compared to recent efforts to build foundation models in astrophysics (e.g., AstroPT (Smith et al. 2024; Euclid Collaboration et al. 2025), AstroCLIP (Parker et al. 2024)), our work adopts a complementary strategy to address data scarcity. While such pretrained models encode compact representations of observed galaxy images through self-supervised learning, their deployment to specific scientific tasks often requires extensive fine-tuning with domain-specific labels.

Here, our framework offers dual synergies: first, by generating high-quality labeled datasets to streamline fine-tuning for targeted applications, and second, by augmenting pretraining itself through synthetic samples that populate underrepresented regions of high-dimensional pixel space (e.g., rare morphologies, extreme physical parameters and instrument systematics). This symbiotic relationship between generative and foundational models promises to accelerate discoveries in data-driven astrophysics.

Despite our diffusion model demonstrating capabilities akin to a world simulator—for example, generating realistic dusty early-type galaxies (D-ETGs) by combining

morphological features from early-type galaxies and disk galaxies with dust lanes—this data-synthetic methodology remains confined to the framework of association modeling. As such, a substantial gap persists between these diffusion models, a challenge that extends even to state-of-the-art video generation models like Sora<sup>3</sup>. By relying solely on associative relationships between observed features, such generative models cannot address counterfactual “what if” questions—for instance, “What would this galaxy look like if traced back to its formation epoch?” or “How would its morphology differ under altered cosmological conditions?” (Pearl 2009, 2010).

As such, we explicitly frame our diffusion model as a surrogate for data augmentation under known feature associations, rather than a tool for physical simulation or causal inference. Its utility lies in expanding the diversity of observable feature combinations within the constraints of existing astronomical knowledge. For questions requiring causal modeling of cosmic processes, complementary physical simulation frameworks—incorporating cosmological evolution and subgrid physics will remain indispensable (e.g., Crain et al. 2015; Nelson et al. 2019).

Looking ahead, generative models like ours are poised to redefine the frontiers of scientific discovery by enabling imaginations at cosmic scales. By synthesizing physi-

<sup>3</sup> <https://openai.com/index/sora/>

cally plausible yet observationally rare phenomena—from extreme galaxy mergers (e.g., Athanassoula & Bosma 2019) to hypothetical Pop III galaxies (e.g., Trussler et al. 2023; Lin et al. 2023b) – these models can serve as hypothesis generators, guiding telescopes toward uncharted regions of parameter space. Furthermore, by blending data-driven synthesis with physical priors, we envision a future where generative models act as collaborative partners in the scientific process—not just filling data gaps, but actively expanding the scope of questions we can ask about the universe.

## 6. CONCLUSIONS

In this study, we propose employing a conditional diffusion model as a surrogate for synthesizing galaxy images. Our research demonstrates that this diffusion model can generate high-fidelity galaxy images, closely adhering to specified morphological conditions while maintaining low computational cost. These synthesized images effectively address the data scarcity issue in astrophysical machine learning training pipelines. As evidenced by our experiments on tasks such as galaxy morphology classification and rare object detection, incorporating these augmented training data into machine learning training pipelines yields tangible scientific benefits. We summarize our contributions as follows:

1. We fine-tuned the pre-trained conditional diffusion model **Stable-Diffusion-v1-5** using high-quality morphology label - galaxy image pairs from the Galaxy Zoo 2 dataset. The fine-tuned model demonstrates excellent performance in synthesizing high-fidelity images that closely follow morphological instructions.
2. We quantitatively evaluated the quality of the generated images from three distinct perspectives: (1) realism (visual fidelity relative to real observations), (2) diversity (morphological variety across outputs), and (3) consistency (adherence to input conditions), thus providing a novel evaluation method for astronomical image simulation. Our results show that after sufficient training, the diffusion model can generate realistic galaxy images that are consistent with input morphology conditions and exhibit diversity. We also explored the trade-off between realism and diversity, which can serve as a valuable reference for future applications.
3. We demonstrated that integrating the synthesized images into machine learning pipelines can improve the purity and completeness of machine learning model performance by up to 30% in classical morphology classification tasks, such as spi-

ral/disk/bar/bulge classification, compared to the baseline. This highlights the model’s potential in overcoming data shortages in machine learning training pipelines.

4. We further demonstrated that our diffusion model functions as a “world simulator” surrogate, enabling generative extrapolation from well-observed galaxies to rare or even unobserved domains. Using early-type galaxies with prominent dust lanes as a test case (accounting for approximately 0.1% of the Galaxy Zoo 2 dataset and excluded from the training data beforehand), we showed that our generative model can successfully synthesize these galaxies and enhance downstream machine learning models. Our model led to 520 additional dusty early-type galaxies from the same dataset, doubling the sample size compared to previous studies, which only reported 352 samples. This newly created catalog holds scientific value as a proxy for studying merger remnants and dust properties.

While state-of-the-art hydrodynamic simulations seek to reproduce the Universe’s formation via first-principle calculations, our focus here is to empirically model it by harnessing the exponential growth of astronomical observational data. By employing conditional diffusion models to generate large quantities of realistic galaxy images, we supply rich, diverse training samples for machine learning (ML) algorithms and bridge gaps in observational datasets.

This framework not only improves the performance of ML models in tasks like galaxy morphology classification and rare object detection but, more crucially, enables scientists to explore physical processes not yet fully understood through generative extrapolation. In doing so, it constructs a novel bridge between theoretical frameworks and observational evidence, accelerating our comprehension of the Universe’s evolution and structural formation through a purely data-driven lens.

## 7. DATA AVAILABILITY

The data used in this study, including the preprocessed Galaxy Zoo 2 (GZ2) dataset<sup>4</sup> and the early-type dust lane galaxy catalog we contributed<sup>5</sup>, are publicly available now. The GZ2 dataset can be accessed at <https://data.galaxyzoo.org/>, which includes morphological classifications of galaxies from the Sloan Digital Sky Survey (SDSS). The early-type dust lane galaxy catalog for comparison is available in Kaviraj et al. (2012).

<sup>4</sup> Training dataset: <https://zenodo.org/records/15669465>

<sup>5</sup> D-ETG catalog: <https://zenodo.org/records/15636756>

The model pipeline in this study is available at <https://github.com/chenruiRae/GalaxySD> and the trained diffusion model weights are available at <https://huggingface.co/CosmosDream/GalaxySD>. For any additional information or specific requests regarding the data or code, please contact the corresponding author.

## 8. AUTHOR CONTRIBUTIONS

CM conducted experimental runs, created scientific visualizations, and contributed to draft revision. ZS oversaw program design, developed code for the embedding model, and led manuscript writing and revision efforts. TJ gave the initial implementation of the diffusion model fine-tuning, participated in scientific discussions, and provided critical suggestions for manuscript refinement. ZC, YST, and SH offered expert scientific and technical guidance, along with constructive feedback on the manuscript. YST additionally contributed to the selection of the D-ETG research topic and the D-ETG catalog. MYL developed the visual inspection program utilized in the analysis.

## 9. ACKNOWLEDGMENTS

ZS and SH acknowledge support from the National Natural Science Foundation of China (Grants No. 12273015 & 12433003) and the China Crewed Space Program through its Space Application System. ML and ZC acknowledge support from the National Key R&D Program of China (grant no. 2023YFA1605600) and Tsinghua University Initiative Scientific Research Program (No. 20223080023). The authors thank Hongming Tang, Yanhan Guo and Huiling Liu for their valuable discussions and constructive comments. We also appreciate the helpful technical feedback provided by [Morph AI Inc.](#) The authors acknowledge the Tsinghua Astrophysics High-Performance Computing platform at Tsinghua University for providing computational and data storage resources that have contributed to the research results reported within this paper.

## APPENDIX

### A. SIMCLR AS A EMBEDDING TOOL FOR GALAXY IMAGE

As our evaluation metric described in Section 4 involves an encoder  $f_\phi : \mathbb{R}^{H \times W \times 3} \rightarrow \mathbb{R}^L$  to map high-dimensional galaxy images into low-dimensional latent representations, we here detail the representation learning technique used in this work – SimCLR here.

SimCLR ([Chen et al. 2020](#)) is a widely-used self-supervised learning technique in computer vision. The core idea behind, named as contrastive learning, is to construct a series positive and negative pair through data augmentation, and then train a neural network to pull together representations of two differently augmented views from the same galaxy image, while simultaneously pushing apart representations from distinct images. This contrastive mechanism drives the encoder to learn invariant features that robustly capture the morphological details of galaxies, thereby creating a highly discriminative embedding space. As a result, the learned representations not only improve the performance in downstream tasks such as image synthesis and classification but also enhance the overall ability to discern subtle astrophysical features. Compared to other representation learning techniques such as masked image modeling (e.g., [Xie et al. 2021](#)) and variational autoencoders (e.g., [Kingma & Welling 2013](#)), contrastive learning balances both model performance and the cost to training the model and already has wide applications in astrophysics (e.g., [Stein et al. 2022](#); [Desmons et al. 2024](#); [Mohale & Lochner 2024](#)).

Formally, let  $\mathbf{x}_i$  be an image of a galaxy, and let  $\mathbf{x}_i^a$  and  $\mathbf{x}_i^b$  be two augmented views of  $\mathbf{x}_i$ . These views form a positive pair  $(\mathbf{x}_i^a, \mathbf{x}_i^b)$ . For a batch of  $N$  images, we generate  $2N$  augmented views, resulting in  $N$  positive pairs and  $2N(2N - 2)$  negative pairs. The goal is to learn an encoder  $f_\phi$  that maps images to a latent space where positive pairs are close and negative pairs are far apart.

The contrastive loss, often referred to as the InfoNCE loss, is defined as:

$$\mathcal{L}_{\text{contrastive}} = - \sum_{i=1}^N \log \frac{\exp(\text{sim}(f_\phi(\mathbf{x}_i^a), f_\phi(\mathbf{x}_i^b))/\tau)}{\sum_{j=1}^{2N} \mathbb{I}_{[j \neq i]} \exp(\text{sim}(f_\phi(\mathbf{x}_i^a), f_\phi(\mathbf{x}_j))/\tau)},$$

where  $\text{sim}(\cdot, \cdot)$  denotes the cosine similarity between two vectors,  $\tau$  is a temperature parameter, and  $\mathbb{I}_{[j \neq i]}$  is an indicator function that is 1 if  $j \neq i$  and 0 otherwise.

By minimizing this loss, the encoder learns to produce representations that are invariant to the augmentations applied to the same galaxy image while being discriminative enough to distinguish between different galaxies. This learned



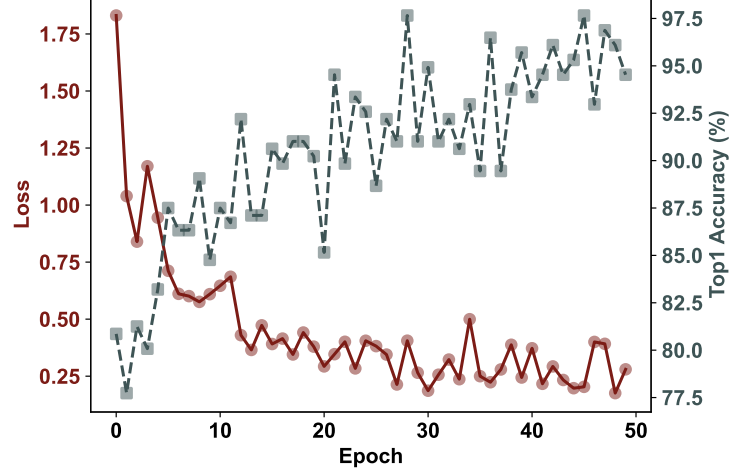


**Figure A1.** The contrastive loss and top-1 accuracy for evaluation along epochs when training SimCLR. Our representation learning model converges stably during the training progress.

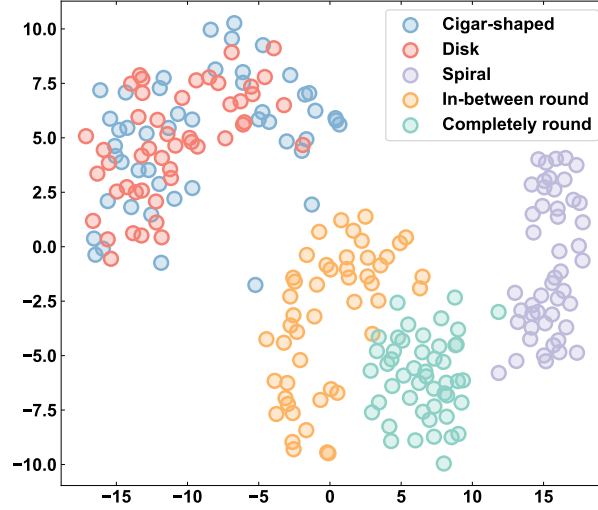


**Figure A2.** t-SNE visualization of the learned embeddings from the SimCLR model. The points are colored by different morphological features as shown in Figure 3. Different morphologies are clearly distinguished within the latent space, demonstrate the effectiveness of our representation learning model.

representation can then be used for various downstream tasks, such as galaxy morphology classification, anomaly detection, and image synthesis, providing a robust foundation for further analysis.

To implement the SimCLR framework, we utilize a ResNet18 architecture as our encoder  $f_\phi$ . ResNet18, a widely-used convolutional neural network, is chosen for its balance between depth and computational efficiency, making it suitable for extracting rich features from galaxy images. The network is initialized with weights pre-trained on ImageNet to leverage transfer learning benefits. We train the model on the Galaxy Zoo dataset, which includes 300,000 annotated galaxy images from the Sloan Digital Sky Survey (SDSS). Each image undergoes a series of augmentations, such as random cropping, flipping, and color jittering, to generate positive pairs. The model is trained for 200 epochs with a batch size of 256 and a learning rate of 0.001, using the Adam optimizer. The temperature parameter  $\tau$  is set to 0.5.

The training process effectively minimizes the contrastive loss, as evidenced by the steady decrease in loss values and the increase in cosine similarity between positive pairs over epochs, as shown in Figure A1. This indicates that the encoder is successfully learning to produce invariant representations for augmented views of the same galaxy image while distinguishing between different galaxies. The t-SNE visualization in Figure A2 further demonstrates that the

learned embeddings form distinct clusters corresponding to different galaxy morphologies, validating the effectiveness of the SimCLR framework in capturing meaningful features. The aim of this training is to create a robust embedding space that can be used to evaluate the quality of generated galaxy images, ensuring that they closely resemble real observations and adhere to the specified morphological conditions.

### B. HIERARCHICAL MORPHOLOGICAL LABELLING SYSTEM IN GZ2

The GZ2 labelling system uses a hierarchical framework starting with broad early/late-type galaxy distinctions, followed by detailed features like bars, dust lanes, and merger signatures. This structured approach enables systematic annotation of both global and fine-grained morphological attributes, as shown in Figure B3.

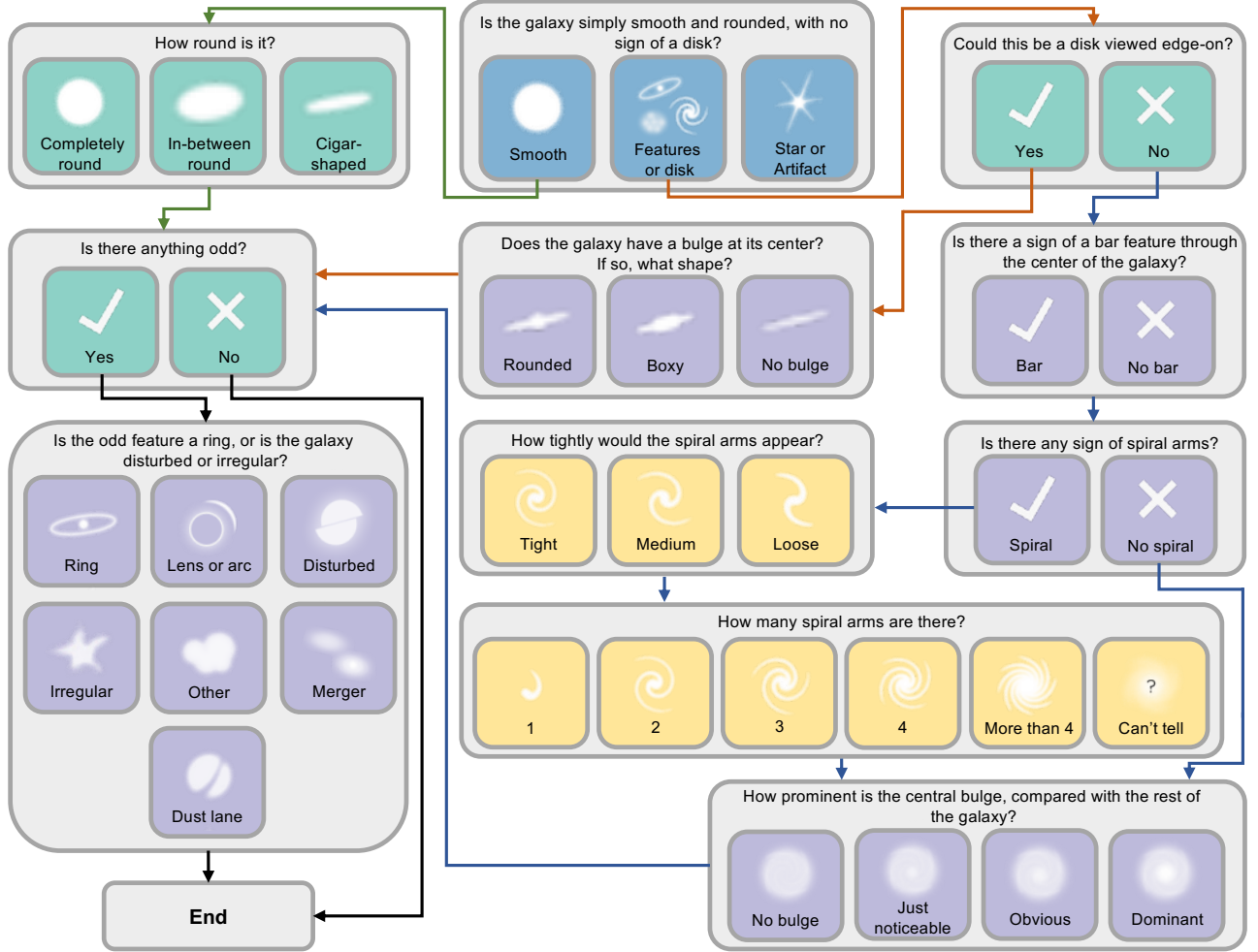


**Figure B3.** The question tree we use to annotate galaxy morphologies was initially proposed by Willett et al. (2013). This hierarchical framework includes both high-level early/late-type classifications and detailed morphological features (e.g., dust, or mergers).

### C. CROSS-ATTENTION MECHANISM IN CONDITIONAL DIFFUSION MODEL

In the diffusion model, conditioning on textual prompts is achieved through a cross-attention mechanism integrated into the U-Net backbone of the denoising process. Instead of conditioning the model via concatenation or direct feature injection, it employs text-image cross-attention mechanism at multiple layers, enabling fine-grained and semantically aligned generation guided by language.

Let  $\mathbf{x}_t \in \mathbb{R}^{C \times H \times W}$  denote the noisy latent representation at timestep  $t$ , and let  $\boldsymbol{\tau} = [\tau_1, \dots, \tau_n]$  represent the embedded text tokens, where each  $\tau_i \in \mathbb{R}^d$  is obtained from a frozen text encoder. The cross-attention module computes output features  $\mathbf{y} \in \mathbb{R}^d$  using the following attention mechanism:

$$\text{Attention}(\mathbf{Q}, \mathbf{K}, \mathbf{V}) = \text{softmax}\left(\frac{\mathbf{Q}\mathbf{K}^\top}{\sqrt{d}}\right) \mathbf{V} \quad (\text{C1})$$

In the cross-attention block, the queries  $\mathbf{Q} \in \mathbb{R}^{hw \times d}$  are derived from the spatial latent features, while the keys  $\mathbf{K} \in \mathbb{R}^{n \times d}$  and values  $\mathbf{V} \in \mathbb{R}^{n \times d}$  come from the encoded text tokens  $\boldsymbol{\tau}$ . This enables spatially-aware modulation of the visual features based on semantic relevance to the text.

The cross-attention is inserted into the U-Net's ResNet blocks as follows:

$$\mathbf{x}_{\text{out}} = \mathbf{x}_{\text{in}} + \text{Attention}(\phi(\mathbf{x}_{\text{in}}), \boldsymbol{\tau}, \boldsymbol{\tau}) \quad (\text{C2})$$

where  $\phi$  denotes a linear projection aligning the latent features to the attention embedding dimension. Multi-head attention (Vaswani et al. 2017) is used to capture diverse semantic relationships between image regions and language concepts.

Applying this mechanism within the U-Net architecture, diffusion model ensures that both local textures and global structure are effectively guided by the input prompt, achieving high-fidelity text-to-image synthesis.

During inference, to enhance targeted morphological features (e.g., dust lanes in this study), we manually assign weights to the corresponding text embeddings to emphasize the desired features, as illustrated in Table 1 and Figure 7. Such enhancement is critical when pushing the boundaries of diffusion models for generative extrapolation tasks.

#### D. ADDITIONAL SANITY CHECK ON OUR D-ETG SAMPLES

We here present the r-band magnitude and stellar mass distribution to complete our discussions in Section 4.3. As we have We present the r-band magnitude and stellar mass distributions to complement our discussions in Section 4.3. Having identified 520 new D-ETGs using ML models enhanced with synthetic images, we compare their properties with the D-ETG sample from Kaviraj et al. (2012) to validate their shared physical consistency and with a control sample of early-type galaxies (ETGs) to ensure rigorous sample control.

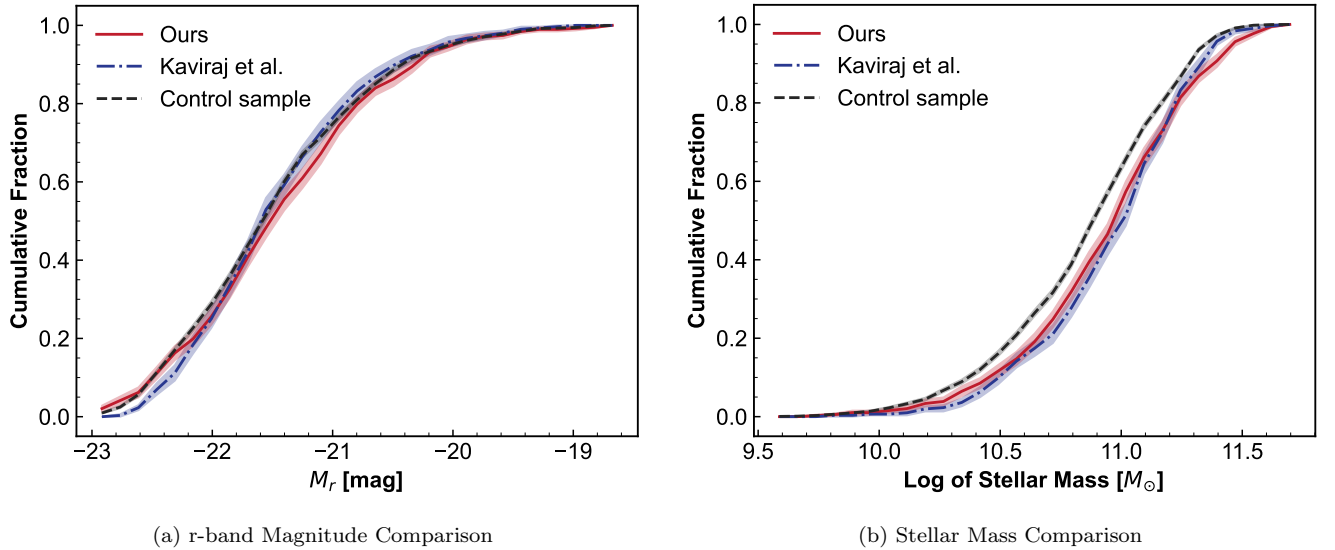


**Figure D4.** Cumulative distribution functions (CDFs) comparing r-band magnitudes and stellar masses of our newly identified D-ETGs (red), the D-ETG sample from Kaviraj et al. (2012) (blue), and control ETGs (black). The close alignment between our sample and Kaviraj et al. (2012) confirms consistent physical properties for dusty early-type galaxies, while systematic differences from control ETGs validate the distinctiveness of the dusty morphology subset and the rigor of our sample control.

### E. COMPARED TO GPT-4O

As we have demonstrated that our fine-tuned diffusion model can generate high-quality galaxy images adhere to instruct we compare our diffusion model's results with the state-of-the-art industrial text-to-image model GPT-4o<sup>6</sup> here, having demonstrated in the main text that our model generates high-fidelity, scientifically meaningful galaxy images. As shown in Figure E5, industrial text-to-image models effectively capture key visual features and morphological concepts of galaxy images but require further refinement to accurately replicate the systematic characteristics of real observational data.

For future astrophysical AI development, leveraging pre-trained industrial generative models as a foundation is more pragmatic. As illustrated in our study, starting from **Stable-Diffusion-v1-5** and training on only 27,910 high-quality annotated galaxy images yielded strong performance. Industrial models, having been trained on billions of high-quality image-text pairs, already encode the majority of general visual concepts, streamlining downstream domain adaptation for specialized astronomical applications.

<sup>6</sup> <https://openai.com/index/introducing-4o-image-generation/>



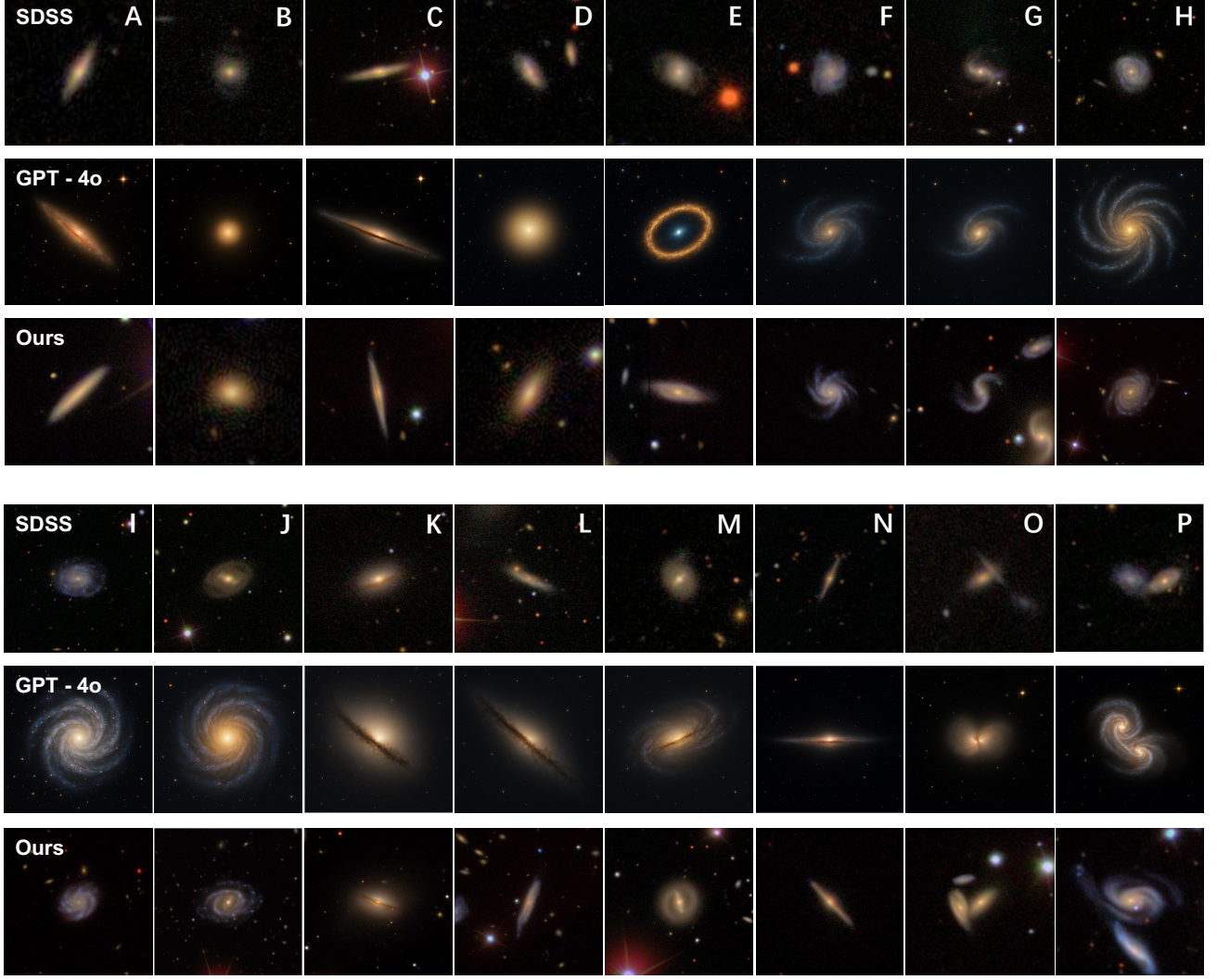


**Figure E5.** Comparison of galaxy images from SDSS, our model’s simulations, and GPT-4o. Annotated capital letters correspond to generation prompts listed in Table 1. While GPT-4o has encode those visual concepts related to galaxy morphology, it may not fully reproduce real observed image characteristics, e.g., noise level and point spread functions. As demonstrated in our study, starting from industrial pre-trained models (e.g., *Stable-Diffusion-v1-5*) and performing domain adaptation on science-specific datasets efficiently bridges this gap, enabling accurate reproduction of observational features critical for astrophysical applications.

## REFERENCES

- Ahn, C. P., Alexandroff, R., Allende Prieto, C., et al. 2014, *The Astrophysical Journal Supplement Series*, 211, 17, doi: [10.1088/0067-0049/211/2/17](https://doi.org/10.1088/0067-0049/211/2/17)
- Andersson, A., Lintott, C., Fender, R., et al. 2024, arXiv e-prints, arXiv:2410.01034, doi: [10.48550/arXiv.2410.01034](https://doi.org/10.48550/arXiv.2410.01034)
- Astolfi, P., Careil, M., Hall, M., et al. 2024, arXiv e-prints, arXiv:2406.10429, doi: [10.48550/arXiv.2406.10429](https://doi.org/10.48550/arXiv.2406.10429)
- Athanassoula, E., & Bosma, A. 2019, *Nature Astronomy*, 3, 588, doi: [10.1038/s41550-019-0822-z](https://doi.org/10.1038/s41550-019-0822-z)
- Azizi, S., Kornblith, S., Saharia, C., Norouzi, M., & Fleet, D. J. 2023, arXiv e-prints, arXiv:2304.08466, doi: [10.48550/arXiv.2304.08466](https://doi.org/10.48550/arXiv.2304.08466)
- Ball, N. M., Brunner, R. J., Myers, A. D., & Tcheng, D. 2006, *The Astrophysical Journal*, 650, 497, doi: [10.1086/507440](https://doi.org/10.1086/507440)
- Banerji, M., Lahav, O., Lintott, C. J., et al. 2010, *Monthly Notices of the Royal Astronomical Society*, 406, 342, doi: [10.1111/j.1365-2966.2010.16713.x](https://doi.org/10.1111/j.1365-2966.2010.16713.x)
- Banfield, J. K., Wong, O. I., Willett, K. W., et al. 2015, *Monthly Notices of the Royal Astronomical Society*, 453, 2326, doi: [10.1093/mnras/stv1688](https://doi.org/10.1093/mnras/stv1688)
- Bezanson, R., Labbe, I., Whitaker, K. E., et al. 2024, *ApJ*, 974, 92, doi: [10.3847/1538-4357/ad66cf](https://doi.org/10.3847/1538-4357/ad66cf)
- Bhaskara, R., Georgakis, G., Nash, J., et al. 2024, arXiv e-prints, arXiv:2401.12414, doi: [10.48550/arXiv.2401.12414](https://doi.org/10.48550/arXiv.2401.12414)
- Bishop, C. M. 2006, *Pattern Recognition and Machine Learning* (Springer)
- Bowles, M., Tang, H., Vardoulaki, E., et al. 2023, *Monthly Notices of the Royal Astronomical Society*, 522, 2584, doi: [10.1093/mnras/stad1021](https://doi.org/10.1093/mnras/stad1021)
- Brownstein, J. R., Bolton, A. S., Schlegel, D. J., et al. 2012, *The Astrophysical Journal*, 744, 41, doi: [10.1088/0004-637X/744/1/41](https://doi.org/10.1088/0004-637X/744/1/41)
- Bruzual, G., & Charlot, S. 2003, *Monthly Notices of the Royal Astronomical Society*, 344, 1000, doi: [10.1046/j.1365-8711.2003.06897.x](https://doi.org/10.1046/j.1365-8711.2003.06897.x)
- Buzzo, M. L., Forbes, D. A., Jarrett, T. H., et al. 2025, *Monthly Notices of the Royal Astronomical Society*, 536, 2536, doi: [10.1093/mnras/stae2700](https://doi.org/10.1093/mnras/stae2700)
- Calzetti, D., Armus, L., Bohlin, R. C., et al. 2000, *The Astrophysical Journal*, 533, 682, doi: [10.1086/308692](https://doi.org/10.1086/308692)
- Campagne, J.-E. 2025, *Monthly Notices of the Royal Astronomical Society*, 539, 3445, doi: [10.1093/mnras/staf533](https://doi.org/10.1093/mnras/staf533)
- Casey, C. M., Kartaltepe, J. S., Drakos, N. E., et al. 2023, *ApJ*, 954, 31, doi: [10.3847/1538-4357/acc2bc](https://doi.org/10.3847/1538-4357/acc2bc)
- Cavuoti, S., Doorenbos, L., De Cicco, D., et al. 2024, arXiv e-prints, arXiv:2411.18206, doi: [10.48550/arXiv.2411.18206](https://doi.org/10.48550/arXiv.2411.18206)
- Chen, Q.-H., Grasha, K., Battisti, A. J., et al. 2023, *MNRAS*, 519, 4801, doi: [10.1093/mnras/stac3790](https://doi.org/10.1093/mnras/stac3790)
- Chen, T., Kornblith, S., Norouzi, M., & Hinton, G. 2020, arXiv e-prints, arXiv:2002.05709, doi: [10.48550/arXiv.2002.05709](https://doi.org/10.48550/arXiv.2002.05709)
- Cho, J., Hu, Y., Garg, R., et al. 2023, arXiv e-prints, arXiv:2310.18235, doi: [10.48550/arXiv.2310.18235](https://doi.org/10.48550/arXiv.2310.18235)
- Ćiprijanović, A., Lewis, A., Pedro, K., et al. 2023, *Machine Learning: Science and Technology*, 4, 025013, doi: [10.1088/2632-2153/acca5f](https://doi.org/10.1088/2632-2153/acca5f)
- Conselice, C. J. 2003, *ApJS*, 147, 1, doi: [10.1086/375001](https://doi.org/10.1086/375001)
- Conselice, C. J., Bershad, M. A., & Jangren, A. 2000, *ApJ*, 529, 886, doi: [10.1086/308300](https://doi.org/10.1086/308300)
- Crain, R. A., Schaye, J., Bower, R. G., et al. 2015, *Monthly Notices of the Royal Astronomical Society*, 450, 1937, doi: [10.1093/mnras/stv725](https://doi.org/10.1093/mnras/stv725)
- Cui, J., Gu, Q., & Shi, Y. 2024, *Monthly Notices of the Royal Astronomical Society*, 528, 2391, doi: [10.1093/mnras/stae156](https://doi.org/10.1093/mnras/stae156)
- Dabbech, A., Terris, M., Jackson, A., et al. 2022, *The Astrophysical Journal*, 939, L4, doi: [10.3847/2041-8213/ac98af](https://doi.org/10.3847/2041-8213/ac98af)
- Dalcanton, J. J., Yoachim, P., & Bernstein, R. A. 2004, *The Astrophysical Journal*, 608, 189, doi: [10.1086/386358](https://doi.org/10.1086/386358)
- Davis, T. A., Rowlands, K., Allison, J. R., et al. 2015, *Monthly Notices of the Royal Astronomical Society*, 449, 3503, doi: [10.1093/mnras/stv597](https://doi.org/10.1093/mnras/stv597)
- Deng, L., Shu, Y., Wang, L., et al. 2025, *The Astrophysical Journal*, 982, L23, doi: [10.3847/2041-8213/adbae5](https://doi.org/10.3847/2041-8213/adbae5)
- Desmons, A., Brough, S., & Lanusse, F. 2024, *Monthly Notices of the Royal Astronomical Society*, 531, 4070, doi: [10.1093/mnras/stae1402](https://doi.org/10.1093/mnras/stae1402)
- Dhariwal, P., & Nichol, A. 2021, arXiv e-prints, arXiv:2105.05233, doi: [10.48550/arXiv.2105.05233](https://doi.org/10.48550/arXiv.2105.05233)
- Duev, D. A., Mahabal, A., Ye, Q., et al. 2019, *Monthly Notices of the Royal Astronomical Society*, 486, 4158, doi: [10.1093/mnras/stz1096](https://doi.org/10.1093/mnras/stz1096)
- Euclid Collaboration, Scaramella, R., Amiaux, J., et al. 2022, *Astronomy and Astrophysics*, 662, A112, doi: [10.1051/0004-6361/202141938](https://doi.org/10.1051/0004-6361/202141938)
- Euclid Collaboration, Siudek, M., Huertas-Company, M., et al. 2025, arXiv e-prints, arXiv:2503.15312, doi: [10.48550/arXiv.2503.15312](https://doi.org/10.48550/arXiv.2503.15312)
- Finkelstein, S. L., Bagley, M. B., Arrabal Haro, P., et al. 2025, *ApJL*, 983, L4, doi: [10.3847/2041-8213/adbbd3](https://doi.org/10.3847/2041-8213/adbbd3)
- Fontanot, F., De Lucia, G., Wilman, D., & Monaco, P. 2011, *MNRAS*, 416, 409, doi: [10.1111/j.1365-2966.2011.19047.x](https://doi.org/10.1111/j.1365-2966.2011.19047.x)
- Foyle, K., Rix, H. W., Walter, F., & Leroy, A. K. 2010, *ApJ*, 725, 534, doi: [10.1088/0004-637X/725/1/534](https://doi.org/10.1088/0004-637X/725/1/534)

- Fraser-McKelvie, A., Merrifield, M., Aragón-Salamanca, A., et al. 2019, *MNRAS*, 488, L6, doi: [10.1093/mnrasl/slz085](https://doi.org/10.1093/mnrasl/slz085)
- Friedli, D., Benz, W., & Kennicutt, R. 1994, *ApJL*, 430, L105, doi: [10.1086/187449](https://doi.org/10.1086/187449)
- Fudamoto, Y., Inoue, A. K., & Sugahara, Y. 2022, *The Astrophysical Journal*, 938, L24, doi: [10.3847/2041-8213/ac982b](https://doi.org/10.3847/2041-8213/ac982b)
- Gao, R., Chen, K., Xiao, B., et al. 2024, arXiv e-prints, arXiv:2411.13807, doi: [10.48550/arXiv.2411.13807](https://doi.org/10.48550/arXiv.2411.13807)
- Gardner, J. P., Mather, J. C., Abbott, R., et al. 2023, *Publications of the Astronomical Society of the Pacific*, 135, 068001, doi: [10.1088/1538-3873/acd1b5](https://doi.org/10.1088/1538-3873/acd1b5)
- Goodfellow, I., Bengio, Y., & Courville, A. 2016, *Deep Learning* (MIT Press)
- Gui, J., Chen, T., Zhang, J., et al. 2023, arXiv e-prints, arXiv:2301.05712, doi: [10.48550/arXiv.2301.05712](https://doi.org/10.48550/arXiv.2301.05712)
- Gupta, A., Yu, L., Sohn, K., et al. 2023, arXiv e-prints, arXiv:2312.06662, doi: [10.48550/arXiv.2312.06662](https://doi.org/10.48550/arXiv.2312.06662)
- Hackstein, S., Kinakh, V., Bailer, C., & Melchior, M. 2023, *Astronomy and Computing*, 42, 100685, doi: [10.1016/j.ascom.2022.100685](https://doi.org/10.1016/j.ascom.2022.100685)
- Hart, R. E., Bamford, S. P., Willett, K. W., et al. 2016, *MNRAS*, 461, 3663, doi: [10.1093/mnras/stw1588](https://doi.org/10.1093/mnras/stw1588)
- Haslbauer, M., Banik, I., Kroupa, P., Wittenburg, N., & Javanmardi, B. 2022, *The Astrophysical Journal*, 925, 183, doi: [10.3847/1538-4357/ac46ac](https://doi.org/10.3847/1538-4357/ac46ac)
- Hausen, R., & Robertson, B. E. 2020, *ApJS*, 248, 20, doi: [10.3847/1538-4365/ab8868](https://doi.org/10.3847/1538-4365/ab8868)
- Hayat, M. A., Stein, G., Harrington, P., Lukić, Z., & Mustafa, M. 2021, *The Astrophysical Journal*, 911, L33, doi: [10.3847/2041-8213/abf2c7](https://doi.org/10.3847/2041-8213/abf2c7)
- He, K., Zhang, X., Ren, S., & Sun, J. 2016, in 2016 IEEE Conference on Computer Vision and Pattern Recognition (CVPR), 1, doi: [10.1109/CVPR.2016.90](https://doi.org/10.1109/CVPR.2016.90)
- Ho, J., Jain, A., & Abbeel, P. 2020, arXiv e-prints, arXiv:2006.11239, doi: [10.48550/arXiv.2006.11239](https://doi.org/10.48550/arXiv.2006.11239)
- Ho, J., Chan, W., Saharia, C., et al. 2022, arXiv e-prints, arXiv:2210.02303, doi: [10.48550/arXiv.2210.02303](https://doi.org/10.48550/arXiv.2210.02303)
- Hood, C. E., Kannappan, S. J., Stark, D. V., et al. 2018, *The Astrophysical Journal*, 857, 144, doi: [10.3847/1538-4357/aab719](https://doi.org/10.3847/1538-4357/aab719)
- Hopkins, P. F., Gurvich, A. B., Shen, X., et al. 2023, *Monthly Notices of the Royal Astronomical Society*, 525, 2241, doi: [10.1093/mnras/stad1902](https://doi.org/10.1093/mnras/stad1902)
- Hopkins, P. F., Bundy, K., Croton, D., et al. 2010, *ApJ*, 715, 202, doi: [10.1088/0004-637X/715/1/202](https://doi.org/10.1088/0004-637X/715/1/202)
- Hu, Y., Liu, B., Kasai, J., et al. 2023, arXiv e-prints, arXiv:2303.11897, doi: [10.48550/arXiv.2303.11897](https://doi.org/10.48550/arXiv.2303.11897)
- Irueta-Goyena, B. Y., Rachith, E., Hellmich, S., et al. 2025, *Astronomy and Astrophysics*, 694, A49, doi: [10.1051/0004-6361/202452756](https://doi.org/10.1051/0004-6361/202452756)
- Ivezić, Ž., Kahn, S. M., Tyson, J. A., et al. 2019, *The Astrophysical Journal*, 873, 111, doi: [10.3847/1538-4357/ab042c](https://doi.org/10.3847/1538-4357/ab042c)
- Kaviraj, S., Ting, Y.-S., Bureau, M., et al. 2012, *Monthly Notices of the Royal Astronomical Society*, 423, 49, doi: [10.1111/j.1365-2966.2012.20957.x](https://doi.org/10.1111/j.1365-2966.2012.20957.x)
- Keerthi-Vasan, G. C., Sheng, S., Jones, T., Choi, C. P., & Sharpnack, J. 2023, *Monthly Notices of the Royal Astronomical Society*, 524, 5368, doi: [10.1093/mnras/stad1709](https://doi.org/10.1093/mnras/stad1709)
- Khalid, A., Brough, S., Martin, G., et al. 2024, *Monthly Notices of the Royal Astronomical Society*, 530, 4422, doi: [10.1093/mnras/stae1064](https://doi.org/10.1093/mnras/stae1064)
- Kim, D.-W., Yeo, D., Bailer-Jones, C. A. L., & Lee, G. 2021, *Astronomy and Astrophysics*, 653, A22, doi: [10.1051/0004-6361/202140369](https://doi.org/10.1051/0004-6361/202140369)
- Kim, E. J., & Brunner, R. J. 2017, *Monthly Notices of the Royal Astronomical Society*, 464, 4463, doi: [10.1093/mnras/stw2672](https://doi.org/10.1093/mnras/stw2672)
- Kingma, D. P., & Welling, M. 2013, arXiv e-prints, arXiv:1312.6114, doi: [10.48550/arXiv.1312.6114](https://doi.org/10.48550/arXiv.1312.6114)
- Kohandel, M., Pallottini, A., Ferrara, A., et al. 2024, *A&A*, 685, A72, doi: [10.1051/0004-6361/202348209](https://doi.org/10.1051/0004-6361/202348209)
- Kreckel, K., Groves, B., Schinnerer, E., et al. 2013, *The Astrophysical Journal*, 771, 62, doi: [10.1088/0004-637X/771/1/62](https://doi.org/10.1088/0004-637X/771/1/62)
- Lanusse, F., Mandelbaum, R., Ravanbakhsh, S., et al. 2021, *Monthly Notices of the Royal Astronomical Society*, 504, 5543, doi: [10.1093/mnras/stab1214](https://doi.org/10.1093/mnras/stab1214)
- Leoni, M., Ishida, E. E. O., Peloton, J., & Möller, A. 2022, *Astronomy and Astrophysics*, 663, A13, doi: [10.1051/0004-6361/202142715](https://doi.org/10.1051/0004-6361/202142715)
- Leung, H. W., & Bovy, J. 2024, *MNRAS*, 527, 1494, doi: [10.1093/mnras/stad3015](https://doi.org/10.1093/mnras/stad3015)
- Li, J., Greene, J. E., Greco, J. P., et al. 2023, *The Astrophysical Journal*, 955, 1, doi: [10.3847/1538-4357/ace829](https://doi.org/10.3847/1538-4357/ace829)
- Li, J., Melchior, P., Hahn, C., & Huang, S. 2024, *The Astronomical Journal*, 167, 16, doi: [10.3847/1538-3881/ad0be4](https://doi.org/10.3847/1538-3881/ad0be4)
- Li, R., Napolitano, N. R., Tortora, C., et al. 2020, *The Astrophysical Journal*, 899, 30, doi: [10.3847/1538-4357/ab9dfa](https://doi.org/10.3847/1538-4357/ab9dfa)
- Lin, L., Li, C., Du, C., et al. 2020, *MNRAS*, 499, 1406, doi: [10.1093/mnras/staa2913](https://doi.org/10.1093/mnras/staa2913)
- Lin, S., Liu, B., Li, J., & Yang, X. 2023a, arXiv e-prints, arXiv:2305.08891, doi: [10.48550/arXiv.2305.08891](https://doi.org/10.48550/arXiv.2305.08891)



- Lin, T.-Y., Goyal, P., Girshick, R., He, K., & Dollár, P. 2017, in *Proceedings of the IEEE international conference on computer vision*, 2980–2988
- Lin, X., Cai, Z., Zou, S., et al. 2023b, *The Astrophysical Journal*, 944, L59, doi: [10.3847/2041-8213/aca1c4](https://doi.org/10.3847/2041-8213/aca1c4)
- Lintott, C. J., Schawinski, K., Slosar, A., et al. 2008, *MNRAS*, 389, 1179, doi: [10.1111/j.1365-2966.2008.13689.x](https://doi.org/10.1111/j.1365-2966.2008.13689.x)
- Liu, T., Quan, Y., Su, Y., et al. 2025, arXiv e-prints, arXiv:2502.16807, doi: [10.48550/arXiv.2502.16807](https://doi.org/10.48550/arXiv.2502.16807)
- Lizarraga, A., Hanchen Jiang, E., Nowack, J., et al. 2024, arXiv e-prints, arXiv:2411.18440, doi: [10.48550/arXiv.2411.18440](https://doi.org/10.48550/arXiv.2411.18440)
- Lotz, J. M., Primack, J., & Madau, P. 2004, *The Astronomical Journal*, 128, 163, doi: [10.1086/421849](https://doi.org/10.1086/421849)
- Ma, G., Huang, H., Yan, K., et al. 2025, arXiv e-prints, arXiv:2502.10248, doi: [10.48550/arXiv.2502.10248](https://doi.org/10.48550/arXiv.2502.10248)
- Masters, K. L., Mosleh, M., Romer, A. K., et al. 2010, *Monthly Notices of the Royal Astronomical Society*, 405, 783, doi: [10.1111/j.1365-2966.2010.16503.x](https://doi.org/10.1111/j.1365-2966.2010.16503.x)
- Metcalf, R. B., Meneghetti, M., Avestruz, C., et al. 2019, *Astronomy and Astrophysics*, 625, A119, doi: [10.1051/0004-6361/201832797](https://doi.org/10.1051/0004-6361/201832797)
- Mohale, K., & Lochner, M. 2024, *Monthly Notices of the Royal Astronomical Society*, 530, 1274, doi: [10.1093/mnras/stae926](https://doi.org/10.1093/mnras/stae926)
- Morales, G., Martínez-Delgado, D., Grebel, E. K., et al. 2018, *Astronomy and Astrophysics*, 614, A143, doi: [10.1051/0004-6361/201732271](https://doi.org/10.1051/0004-6361/201732271)
- Nedkova, K. V., Häußler, B., Marchesini, D., et al. 2024, *MNRAS*, 532, 3747, doi: [10.1093/mnras/stae1702](https://doi.org/10.1093/mnras/stae1702)
- Neeleman, M., Prochaska, J. X., Kanekar, N., & Rafelski, M. 2020, *Nature*, 581, 269, doi: [10.1038/s41586-020-2276-y](https://doi.org/10.1038/s41586-020-2276-y)
- Nelson, D., Springel, V., Pillepich, A., et al. 2019, *Computational Astrophysics and Cosmology*, 6, 2, doi: [10.1186/s40668-019-0028-x](https://doi.org/10.1186/s40668-019-0028-x)
- Nelson, E. J., Suess, K. A., Bezanson, R., et al. 2023, *ApJL*, 948, L18, doi: [10.3847/2041-8213/acc1e1](https://doi.org/10.3847/2041-8213/acc1e1)
- Noll, S., Burgarella, D., Giovannoli, E., et al. 2009, *Astronomy and Astrophysics*, 507, 1793, doi: [10.1051/0004-6361/200912497](https://doi.org/10.1051/0004-6361/200912497)
- NVIDIA, :, Agarwal, N., et al. 2025, arXiv e-prints, arXiv:2501.03575, doi: [10.48550/arXiv.2501.03575](https://doi.org/10.48550/arXiv.2501.03575)
- O’Brian, T., Ting, Y.-S., Fabbro, S., et al. 2021, *ApJ*, 906, 130, doi: [10.3847/1538-4357/abca96](https://doi.org/10.3847/1538-4357/abca96)
- Omori, K. C., Bottrell, C., Walmsley, M., et al. 2023, *Astronomy and Astrophysics*, 679, A142, doi: [10.1051/0004-6361/202346743](https://doi.org/10.1051/0004-6361/202346743)
- Ono, V., Park, C. F., Mudur, N., et al. 2024, *ApJ*, 970, 174, doi: [10.3847/1538-4357/ad5957](https://doi.org/10.3847/1538-4357/ad5957)
- O’Riordan, C. M., Oldham, L. J., Nersesian, A., et al. 2025, *Astronomy and Astrophysics*, 694, A145, doi: [10.1051/0004-6361/202453014](https://doi.org/10.1051/0004-6361/202453014)
- Parker, L., Lanusse, F., Golkar, S., et al. 2024, *MNRAS*, 531, 4990, doi: [10.1093/mnras/stae1450](https://doi.org/10.1093/mnras/stae1450)
- Pearce-Casey, R., Nagam, B. C., Wilde, J., et al. 2024, arXiv e-prints, arXiv:2411.16808, doi: [10.48550/arXiv.2411.16808](https://doi.org/10.48550/arXiv.2411.16808)
- Pearl, J. 2009, *Causality* (Cambridge: Cambridge University Press)
- . 2010, *International Journal of Biostatistics*, 6, Article 7, doi: [10.2202/1557-4679.1203](https://doi.org/10.2202/1557-4679.1203)
- Pearson, W. J., Santos, D. J. D., Goto, T., et al. 2024, *A&A*, 686, A94, doi: [10.1051/0004-6361/202349034](https://doi.org/10.1051/0004-6361/202349034)
- Planck Collaboration, Aghanim, N., Akrami, Y., et al. 2020, *A&A*, 641, A6, doi: [10.1051/0004-6361/201833910](https://doi.org/10.1051/0004-6361/201833910)
- Pruzhinskaya, M. V., Ishida, E. E. O., Novinskaya, A. K., et al. 2023, *Astronomy and Astrophysics*, 672, A111, doi: [10.1051/0004-6361/202245172](https://doi.org/10.1051/0004-6361/202245172)
- Riggi, S., Cecconello, T., Palazzo, S., et al. 2024, *Publications of the Astronomical Society of Australia*, 41, e085, doi: [10.1017/pasa.2024.84](https://doi.org/10.1017/pasa.2024.84)
- Robertson, B. E., Tacchella, S., Johnson, B. D., et al. 2023, *The Astrophysical Journal*, 942, L42, doi: [10.3847/2041-8213/aca086](https://doi.org/10.3847/2041-8213/aca086)
- Rombach, R., Blattmann, A., Lorenz, D., Esser, P., & Ommer, B. 2021, arXiv e-prints, arXiv:2112.10752, doi: [10.48550/arXiv.2112.10752](https://doi.org/10.48550/arXiv.2112.10752)
- Ronneberger, O., Fischer, P., & Brox, T. 2015, arXiv e-prints, arXiv:1505.04597, doi: [10.48550/arXiv.1505.04597](https://doi.org/10.48550/arXiv.1505.04597)
- Rouhiainen, A., Münchmeyer, M., Shiu, G., Gira, M., & Lee, K. 2024, *Physical Review D*, 109, 123536, doi: [10.1103/PhysRevD.109.123536](https://doi.org/10.1103/PhysRevD.109.123536)
- Rowe, B. T. P., Jarvis, M., Mandelbaum, R., et al. 2015, *Astronomy and Computing*, 10, 121, doi: [10.1016/j.ascom.2015.02.002](https://doi.org/10.1016/j.ascom.2015.02.002)
- Rutherford, T. H., van de Sande, J., Croom, S. M., et al. 2024, *Monthly Notices of the Royal Astronomical Society*, 529, 810, doi: [10.1093/mnras/stae398](https://doi.org/10.1093/mnras/stae398)
- Salim, S., Lee, J. C., Janowiecki, S., et al. 2016, *The Astrophysical Journal Supplement Series*, 227, 2, doi: [10.3847/0067-0049/227/1/2](https://doi.org/10.3847/0067-0049/227/1/2)
- Schinnerer, E., Meidt, S. E., Colombo, D., et al. 2017, *ApJ*, 836, 62, doi: [10.3847/1538-4357/836/1/62](https://doi.org/10.3847/1538-4357/836/1/62)
- Sether, T., Giusarma, E., & Reyes-Hurtado, M. 2024, arXiv e-prints, arXiv:2412.05131, doi: [10.48550/arXiv.2412.05131](https://doi.org/10.48550/arXiv.2412.05131)
- Shabala, S. S., Ting, Y.-S., Kaviraj, S., et al. 2012, *Monthly Notices of the Royal Astronomical Society*, 423, 59, doi: [10.1111/j.1365-2966.2012.20598.x](https://doi.org/10.1111/j.1365-2966.2012.20598.x)



- Slijepcevic, I. V., Scaife, A. M. M., Walmsley, M., et al. 2022, *Monthly Notices of the Royal Astronomical Society*, 514, 2599, doi: [10.1093/mnras/stac1135](https://doi.org/10.1093/mnras/stac1135)
- Smith, M. J., Geach, J. E., Jackson, R. A., et al. 2022, *Monthly Notices of the Royal Astronomical Society*, 511, 1808, doi: [10.1093/mnras/stac130](https://doi.org/10.1093/mnras/stac130)
- Smith, M. J., Roberts, R. J., Angeloudi, E., & Huertas-Company, M. 2024, arXiv e-prints, arXiv:2405.14930, doi: [10.48550/arXiv.2405.14930](https://doi.org/10.48550/arXiv.2405.14930)
- Song, Y., Sohl-Dickstein, J., Kingma, D. P., et al. 2020, arXiv e-prints, arXiv:2011.13456, doi: [10.48550/arXiv.2011.13456](https://doi.org/10.48550/arXiv.2011.13456)
- Song, Z., He, Z., Li, X., et al. 2023, arXiv e-prints, arXiv:2304.12205, doi: [10.48550/arXiv.2304.12205](https://doi.org/10.48550/arXiv.2304.12205)
- Speagle, J. S., Leauthaud, A., Huang, S., et al. 2019a, *MNRAS*, 490, 5658, doi: [10.1093/mnras/stz2968](https://doi.org/10.1093/mnras/stz2968)
- . 2019b, *MNRAS*, 490, 5658, doi: [10.1093/mnras/stz2968](https://doi.org/10.1093/mnras/stz2968)
- Stein, G., Blaum, J., Harrington, P., Medan, T., & Lukić, Z. 2022, *The Astrophysical Journal*, 932, 107, doi: [10.3847/1538-4357/ac6d63](https://doi.org/10.3847/1538-4357/ac6d63)
- Sun, B., Calzetti, D., & Battisti, A. J. 2024a, *ApJ*, 973, 137, doi: [10.3847/1538-4357/ad6157](https://doi.org/10.3847/1538-4357/ad6157)
- Sun, Z., Speagle, J. S., Huang, S., Ting, Y.-S., & Cai, Z. 2023a, arXiv e-prints, arXiv:2310.20125, doi: [10.48550/arXiv.2310.20125](https://doi.org/10.48550/arXiv.2310.20125)
- Sun, Z., Ting, Y.-S., & Cai, Z. 2023b, *The Astrophysical Journal Supplement Series*, 269, 4, doi: [10.3847/1538-4365/acf2f1](https://doi.org/10.3847/1538-4365/acf2f1)
- Sun, Z., Ting, Y.-S., Liang, Y., et al. 2024b, arXiv e-prints, arXiv:2409.14807, doi: [10.48550/arXiv.2409.14807](https://doi.org/10.48550/arXiv.2409.14807)
- Sutton, R. S., & Barto, A. G. 2018, *Reinforcement Learning: An Introduction* (Cambridge, MA, USA: A Bradford Book)
- Sweere, S. F., Valtchanov, I., Lieu, M., et al. 2022, *Monthly Notices of the Royal Astronomical Society*, 517, 4054, doi: [10.1093/mnras/stac2437](https://doi.org/10.1093/mnras/stac2437)
- Tang, H., Scaife, A. M. M., Wong, O. I., et al. 2020, *Monthly Notices of the Royal Astronomical Society*, 499, 68, doi: [10.1093/mnras/staa2805](https://doi.org/10.1093/mnras/staa2805)
- Tanoglidis, D., Čiprijanović, A., Drlica-Wagner, A., et al. 2022, *Astronomy and Computing*, 39, 100580, doi: [10.1016/j.ascom.2022.100580](https://doi.org/10.1016/j.ascom.2022.100580)
- Tenachi, W., Ibata, R., & Diakogiannis, F. I. 2023, *The Astrophysical Journal*, 959, 99, doi: [10.3847/1538-4357/ad014c](https://doi.org/10.3847/1538-4357/ad014c)
- Terris, M., Dabbech, A., Tang, C., & Wiaux, Y. 2023, *Monthly Notices of the Royal Astronomical Society*, 518, 604, doi: [10.1093/mnras/stac2672](https://doi.org/10.1093/mnras/stac2672)
- Thuruthipilly, H., Junais, Koda, J., et al. 2025, arXiv e-prints, arXiv:2502.03142, doi: [10.48550/arXiv.2502.03142](https://doi.org/10.48550/arXiv.2502.03142)
- Ting, Y.-S., Conroy, C., Rix, H.-W., & Cargile, P. 2019, *The Astrophysical Journal*, 879, 69, doi: [10.3847/1538-4357/ab2331](https://doi.org/10.3847/1538-4357/ab2331)
- Trussler, J. A. A., Conselice, C. J., Adams, N. J., et al. 2023, *Monthly Notices of the Royal Astronomical Society*, 525, 5328, doi: [10.1093/mnras/stad2553](https://doi.org/10.1093/mnras/stad2553)
- van Engelen, J. E., & Hoos, H. H. 2020, *Machine Learning*, 109, 373, doi: [10.1007/s10994-019-05855-6](https://doi.org/10.1007/s10994-019-05855-6)
- Vaswani, A., Shazeer, N., Parmar, N., et al. 2017, *Advances in neural information processing systems*, 30
- Vavilova, I. B., Dobrycheva, D. V., Vasylenko, M. Y., et al. 2021, *Astronomy and Astrophysics*, 648, A122, doi: [10.1051/0004-6361/202038981](https://doi.org/10.1051/0004-6361/202038981)
- Villaescusa-Navarro, F., Anglés-Alcázar, D., Genel, S., et al. 2021, *ApJ*, 915, 71, doi: [10.3847/1538-4357/abf7ba](https://doi.org/10.3847/1538-4357/abf7ba)
- Vičánek Martínez, T., Baron Perez, N., & Brüggén, M. 2024, *Astronomy and Astrophysics*, 691, A360, doi: [10.1051/0004-6361/202451429](https://doi.org/10.1051/0004-6361/202451429)
- Walmsley, M., Géron, T., Kruk, S., et al. 2023a, *Monthly Notices of the Royal Astronomical Society*, 526, 4768, doi: [10.1093/mnras/stad2919](https://doi.org/10.1093/mnras/stad2919)
- Walmsley, M., Slijepcevic, I., Bowles, M. R., & Scaife, A. 2022, in *Machine Learning for Astrophysics*, 29, doi: [10.48550/arXiv.2206.11927](https://doi.org/10.48550/arXiv.2206.11927)
- . 2023b, *MNRAS*, 526, 4768, doi: [10.1093/mnras/stad2919](https://doi.org/10.1093/mnras/stad2919)
- Walmsley, M., Bowles, M., Scaife, A. M. M., et al. 2024, arXiv e-prints, arXiv:2404.02973, doi: [10.48550/arXiv.2404.02973](https://doi.org/10.48550/arXiv.2404.02973)
- Wang, B., Zou, J., Cai, Z., et al. 2022, *The Astrophysical Journal Supplement Series*, 259, 28, doi: [10.3847/1538-4365/ac4504](https://doi.org/10.3847/1538-4365/ac4504)
- Wei, L., Huang, S., Li, J., et al. 2025, arXiv e-prints, arXiv:2505.14073, doi: [10.48550/arXiv.2505.14073](https://doi.org/10.48550/arXiv.2505.14073)
- Wei, S., Li, Y., Lu, W., et al. 2022, *Publications of the Astronomical Society of the Pacific*, 134, 114508, doi: [10.1088/1538-3873/aca04e](https://doi.org/10.1088/1538-3873/aca04e)
- Willett, K. W., Lintott, C. J., Bamford, S. P., et al. 2013, *MNRAS*, 435, 2835, doi: [10.1093/mnras/stt1458](https://doi.org/10.1093/mnras/stt1458)
- Willett, K. W., Galloway, M. A., Bamford, S. P., et al. 2017, *MNRAS*, 464, 4176, doi: [10.1093/mnras/stw2568](https://doi.org/10.1093/mnras/stw2568)
- Wittenburg, N., Kroupa, P., Banik, I., Candlish, G., & Samaras, N. 2023, *Monthly Notices of the Royal Astronomical Society*, 523, 453, doi: [10.1093/mnras/stad1371](https://doi.org/10.1093/mnras/stad1371)
- Xie, Z., Zhang, Z., Cao, Y., et al. 2021, arXiv e-prints, arXiv:2111.09886, doi: [10.48550/arXiv.2111.09886](https://doi.org/10.48550/arXiv.2111.09886)
- Xu, C., McCully, C., Dong, B., Howell, D. A., & Sen, P. 2023, *The Astrophysical Journal*, 942, 73, doi: [10.3847/1538-4357/ac9d91](https://doi.org/10.3847/1538-4357/ac9d91)

- Yan, H., Sun, B., & Ling, C. 2024, *ApJ*, 975, 44, doi: [10.3847/1538-4357/ad7de9](https://doi.org/10.3847/1538-4357/ad7de9)
- Yang, X., Mo, H. J., van den Bosch, F. C., Zhang, Y., & Han, J. 2012, *The Astrophysical Journal*, 752, 41, doi: [10.1088/0004-637X/752/1/41](https://doi.org/10.1088/0004-637X/752/1/41)
- Yang, X., Song, Z., King, I., & Xu, Z. 2021, arXiv e-prints, arXiv:2103.00550, doi: [10.48550/arXiv.2103.00550](https://doi.org/10.48550/arXiv.2103.00550)
- Zhan, X., Wang, Q., Huang, K.-h., et al. 2022, arXiv e-prints, arXiv:2203.13450, doi: [10.48550/arXiv.2203.13450](https://doi.org/10.48550/arXiv.2203.13450)
- Zhang, H., & Brandt, T. D. 2021, *The Astronomical Journal*, 162, 139, doi: [10.3847/1538-3881/ac1348](https://doi.org/10.3847/1538-3881/ac1348)
- Zhang, K., & Bloom, J. S. 2020, *The Astrophysical Journal*, 889, 24, doi: [10.3847/1538-4357/ab3fa6](https://doi.org/10.3847/1538-4357/ab3fa6)
- Zhang, P., Yin, H., Li, C., & Xie, X. 2024, arXiv e-prints, arXiv:2403.08381, doi: [10.48550/arXiv.2403.08381](https://doi.org/10.48550/arXiv.2403.08381)
- Zhao, X., Ting, Y.-S., Diao, K., & Mao, Y. 2023, *Monthly Notices of the Royal Astronomical Society*, 526, 1699, doi: [10.1093/mnras/stad2778](https://doi.org/10.1093/mnras/stad2778)
- Zhu, Z., Zhao, H., He, H., et al. 2023, arXiv e-prints, arXiv:2311.01223, doi: [10.48550/arXiv.2311.01223](https://doi.org/10.48550/arXiv.2311.01223)
- Zhuang, F., Qi, Z., Duan, K., et al. 2019, arXiv e-prints, arXiv:1911.02685, doi: [10.48550/arXiv.1911.02685](https://doi.org/10.48550/arXiv.1911.02685)